Atypical B cells mediate poor response to Bacillus Calmette Guérin immunotherapy in non-muscle invasive bladder cancer

Priyanka Yolmo‡[1,2], Sadaf Rahimi‡[1,2], Stephen Chenard[1,2], Gwenaëlle Conseil[1,2], Danielle Jenkins[3], Kartik Sachdeva[1,2], Isaac Emon[1,2], Jake Hamilton[1], Minqi Xu[3], Manu Rangachari[4], Eva Michaud[5], Jose Mansure[5], Wassim Kassouf[5], David M. Berman[2,3], D. Robert Siemens[1,2,6], Madhuri Koti*[1,2]

[1]Department of Biomedical and Molecular Sciences, Queen's University, Kingston, ON, Canada; [2]Cancer Research Institute, Queen's University, Kingston, ON, Canada; [3]Pathology and Molecular Medicine, Queen's University, Kingston, ON, Canada; [4]Department of Molecular Medicine, Faculty of Medicine, Université Laval, Quebec City, QC, Canada; [5]Department of Surgery (Urology) McGill University Health Center; [6]Department of Urology, Queen's University, Kingston, ON, Canada.

Key words: Atypical B cells, Tertiary lymphoid structures, NMIBC, BCG immunotherapy, Sex differences, Four-core genotype

‡**Equal Contribution**

***To whom correspondence should be addressed**

e-mail: kotim@queensu.ca

Abstract

Poor response to Bacillus Calmette-Guérin (BCG) immunotherapy remains a major barrier in the management of patients with non-muscle-invasive bladder cancer (NMIBC). Among the multiple factors contributing to poor outcomes, a B cell infiltrated pre-treatment immune microenvironment of NMIBC tumors has emerged as a key determinant of response to BCG. The mechanisms underlying the paradoxical roles of B cells in NMIBC are poorly understood. Here, we show that B cell dominant tertiary lymphoid structures (TLSs), a hallmark feature of chronic mucosal immune response, are abundant and located close to the epithelial compartment in pre-treatment tumors from BCG non-responders. Digital spatial proteomic profiling of whole tumor sections revealed higher expression of immune exhaustion-associated proteins within the TLSs from both responders and non-responders. Chronic local inflammation, induced by the N-butyl-N-(4-hydroxybutyl) nitrosamine (BBN) carcinogen, led to TLS formation with recruitment and differentiation of the immunosuppressive atypical B cell (ABCs) subset within the bladder microenvironment, predominantly in aging female mice compared to their male counterparts. Depletion of ABCs simultaneous to BCG treatment delayed cancer progression in female mice. Our findings provide the first evidence indicating the role of ABCs in BCG response and will inform future development of therapies targeting the B cell exhaustion axis.

42 **Introduction**

43 Bladder cancer is the most common urological malignancy known worldwide with 573,278 cases
44 diagnosed in 2020[1]. The majority of bladder cancer patients (75-85%) are diagnosed with early-
45 stage NMIBC with a median age at diagnosis of 73 years. Exposure to environmental and
46 occupational carcinogens, tobacco smoking, recurrent urinary tract infections, and aging can be
47 attributed as the major risk factors for bladder cancer.[2] Although more common in males,[3]
48 females with bladder cancer generally present with advanced-stage tumors and experience
49 shorter recurrence-, and progression-free survival[4-7]. Following transurethral resection of
50 bladder tumor (TURBT), patients categorized as intermediate or high-risk NMIBC are treated with
51 intravesical Bacillus Calmette-Guérin (BCG) immunotherapy[8]. The treatment regimen involves an
52 induction phase of 6 weekly instillations after tumor resection, followed by a maintenance phase
53 of 3 weekly instillations every 3-6 months for over 1-3 years depending on the risk stratification[9].
54 BCG treatment in NMIBC patients is linked to a decreased risk of recurrence and progression
55 when compared to transurethral resection alone. Despite its proven efficacy, recurrence post-
56 BCG treatment occurs in over 50% of patients, necessitating repeated treatments, continuous
57 surveillance, and cystectomy upon progression to muscle-invasive stage[10,11].

58

59 Our previous study discovered a significant association between increased density of intra-
60 tumoral B cells and poor outcomes in patients with NMIBC[12]. Tumor-infiltrating B cells are mainly
61 localized within stromal aggregates of immune cells called tertiary lymphoid structures (TLSs)[13].
62 TLS formation in the bladder mucosa is induced due to chronic inflammation,[14] such as persistent
63 urinary tract infection[15,16]; exposure to carcinogens or smoking; immunomodulatory therapy[13];
64 or age-related increase in systemic levels of tumor necrosis factor-α (TNF-α)[17,18]. Indeed, our
65 previous report established an increase in TLS density and maturation with advanced stages of
66 bladder cancer[19].

67

68 Simultaneous to biological aging-associated decline in the periphery, B cell proportions
69 significantly increase at mucosal sites, predominantly within mucosa-associated TLSs[17,20-24].
70 Biological aging, repeated vaccination, and chronic inflammation also lead to the expansion of a

71 circulating B cell subset known as atypical B cells (ABCs). ABCs are observed at a significantly
72 higher frequency in females compared to males, exhibit features of high self-reactivity, and are
73 equipped with specialized antigen-presenting ability[24-28]. In addition, ABCs are known to produce
74 high levels of IL-6 and TNF-α and augment the suppression of B cell lymphopoiesis[29-31]. In aging
75 mice, ABCs increase in the bone marrow with a more pronounced expansion in the spleen,
76 produce autoantibodies and respond uniquely to innate/microbial stimuli[26,32]. A key feature of
77 ABCs is their proliferative response to stimuli that activate endosomal nucleic acid sensing
78 pathways (toll-like receptors; TLR7/9) leading to the production of immunosuppressive cytokines
79 such as IL-10[26,33-36].
80
81 Following intravesical instillation, BCG antigens are internalized by residual cancer cells, normal
82 urothelial cells, and immune cells, leading to immune activation *via* various cytosolic and cell
83 surface receptors such as TLR2/9[36-38]. We hypothesized that repeated local exposure to BCG
84 during the induction phase of the treatment, potentiates systemic expansion of ABCs and
85 recruitment to the bladder. Local immunosuppression mediated by ABCs potentially contributes
86 to disease progression. In this study, we first characterized TLSs in pre-treatment tumors from
87 patients, categorized as BCG responders and non-responders, using multiplex
88 immunofluorescence (mIF) and NanoString GeoMx digital spatial technology (DSP). Since B
89 cells/ABCs exhibit a sex and age-dependent expansion and response to persistent immune
90 activation, we further investigated the potential role of ABCs in BBN carcinogen (mimicking
91 carcinogen present in tobacco smoking) exposed aging wild type C57BL/6 and the four-core
92 genotype (FCG) mice treated with BCG. Overall, our study is the first to demonstrate the
93 expansion of ABCs following chronic carcinogen exposure and repeated BCG immunotherapy as
94 one of the underlying factors for poor response to BCG immunotherapy, specifically, in females.
95
96 **RESULTS**
97 **Pre-treatment tumor adjacent TLSs are increased in BCG non-responders and express proteins**
98 **reflective of immune exhaustion**
99

100 Based on our previous observation of high stromal B cell density and its association with early
101 recurrence and progression, we questioned whether pre-treatment TLSs (characterized by
102 CD79a+ B cells, CD3+ and CD8+ T cells, CD208+ mature dendritic cells (DCs), CD21+ follicular DCs
103 and PNAd+ high endothelial venules) associate with response to BCG. Histopathological
104 evaluation of BCG-naïve whole tumor sections from 28 patients (clinical details in **Suppl. Table**
105 **S1**), revealed the presence of both small and large immune cell aggregates within the lamina
106 propria, indicative of chronic inflammation in the bladder mucosa (**Fig. 1A**). To determine the
107 maturation stage of TLSs, we performed mIF staining, which revealed varying organization and
108 maturation stages of TLSs within the tumors from both BCG responders and non-responders (**Fig.**
109 **1B**). Overall, lymphoid aggregates and mature TLSs (with PNAd+ high endothelial venules,
110 CD21+CD208+ DCs) were higher in whole tumor sections from BCG non-responders compared to
111 responders (**Fig. 1C**).
112
113 Given the counterintuitive finding on the association of TA-TLSs with early recurrence, we further
114 characterized the expression of 49 immune function related proteins (**Suppl. Table S2)** in TLSs
115 from a subset of 12 specimens (6 in each group of responders and non-responders; **Fig. 1D**) using
116 NanoString GeoMx DSP technology **(Fig. S1)**. The area of mature TLSs was higher compared to
117 all other lymphoid aggregates in the lamina propria (**Fig. 1E**). We did not find any statistically
118 significant differences in the expression levels of proteins associated with immune regulatory
119 functions between TLSs from the responders and non-responders. However, when compared to
120 the tumor epithelial compartment, TLSs from both responders and non-responders exhibited
121 statistically significant higher expression of a) immune regulatory proteins such as CD25, ICOS,
122 TIM3, VISTA, PD-L2, IDO-1; b) antigen presentation associated proteins such as B2M, CD11c,
123 CD40; and c) immune cell phenotype associated proteins, CD45, CD20, CD3, CD4, CD56 and CD68
124 (**Fig. 1F**). These findings suggest that pre-treatment TLSs in the bladder microenvironment
125 represent chronic carcinogen induced mucosal inflammation and harbor exhausted populations
126 of immune cells at the time of TURBT.
127

128 **Chronic exposure to BBN carcinogen increases infiltration of atypical B cells within the bladder**
129 **microenvironment**
130
131 To confirm the previously reported age/sex-related shifts in B cell subsets, we first determined
132 the profiles of total B cells and ABCs in the spleen and bone marrow of healthy 12-month-old
133 (reflecting immune profiles of middle-aged humans[18]) C57BL/6 female and male mice. We did
134 not observe any significant differences in the frequency of total B cells (B220+CD19+) from both
135 the spleen and bone marrow of female mice compared to male mice (**Fig. 2A)**; however, splenic
136 ABCs (CD21-/low CD11c+) were significantly higher in 12-month-old female mice compared to
137 their male counterparts (**Fig. 2B – 2D**). Optimization of the B cell-depletion protocol, as per
138 previous reports,[39] was conducted prior to conducting studies in the carcinogen exposed mice
139 (**Fig. S2B)**.
140
141 To determine whether long-term BBN induced genotoxicity and local inflammation leads to
142 increased recruitment of ABCs in the bladder microenvironment, we exposed 12-month-old
143 aging female and male mice to BBN carcinogen for 12 weeks with or without B cell depletion
144 treatment[40]. To specifically determine cause and effect, we first assessed whether B cell
145 depletion during BBN exposure attenuates inflammation in the bladder and delays cancer
146 progression. Results from both local and systemic immune profiling revealed clear sex
147 differences. Female mice displayed an increased frequency of splenic total B cells and ABCs
148 despite depletion **(Fig. 2E and 2F)**. A higher density of ABCs, located with stromal lymphoid
149 aggregates, was observed in the bladder microenvironment of female mice compared to their
150 male counterparts at this time point (**Fig. 2G**). Spatial immune profiling of the bladders collected
151 1 week post last anti-CD20 injection (12 weeks post BBN initiation), revealed significantly fewer
152 numbers of total B cells and ABCs in the B cell-depleted mice in comparison to the B cell-intact
153 mice (**Fig. 2G and 2H**). Histopathological assessment of whole bladder sections from B cell-
154 depleted and B cell intact mice, revealed a benign or close to normal histology of the bladder
155 urothelium in the B cell-depleted female mice **(Fig. S3A**). Reactive atypia/dysplasia was present
156 in the majority of BBN exposed female and male mice that did not undergo any depletion.

157 Importantly this effect was captured at this time point only in the female mice. These findings
158 suggest increased recruitment (or differentiation) of B cells to the bladder microenvironment due
159 to chronic carcinogen induced mucosal inflammation.
160
161 **BBN and BCG induced expansion of splenic ABCs and bladder-associated TLS formation is age**
162 **and sex-dependent**
163
164 To determine the role of B cells in treatment response, we treated BBN exposed mice with three
165 weekly intravesical instillations of BCG (**Fig. 3A**). Compared to healthy bladders (pre-BBN; **Fig.**
166 **3B**), on hematoxylin and eosin (H&E) staining of bladder sections we observed increased
167 infiltration of immune cells and TLSs at 7 weeks post BBN initiation in the bladder lamina propria
168 of female mice (**Fig. 3C**) in contrast to their male counterparts (**Fig. S3D**). Following the 1st dose
169 of BCG, we observed recovery of the urothelium to its benign morphological states (**Fig. 3D**), in
170 contrast to the saline treated mice where dysplasia/CIS like features were still present at this
171 time point (**Fig. S3B**). However, at 1-, 6-, and 8-weeks post completion of all 3 doses of BCG, we
172 observed urothelial dysplasia and progressive focal to widespread CIS, invasive carcinoma-like
173 changes, or papillary tumors despite removal of BBN exposure at the initiation of BCG treatment
174 in female mice (**Fig**. **3E-3G**). Repeated BCG treatments also led to the formation of TLSs, as
175 confirmed by mIF staining, in contrast to the bladders from saline treated mice where tumor
176 growth was observed with no evidence of TLS formation, (**Fig. S3D and S3E**). An increase in
177 splenic ABCs at 1 week post 1st BCG, compared to the pre-BCG levels, was observed in both
178 female and male mice (**Fig. 3H and 3I**). However, the magnitude of increase was significantly
179 higher in female mice (**Fig. 3I**)**.** A significant decline in the proportion of splenic ABCs post 3rd BCG
180 in both sexes suggests its potential trafficking to the bladder mucosa **(Fig. 3I)**. Additionally,
181 histopathological evaluation **(Fig. 3E)** and mIF **(Fig. 3J and 3K)** of the bladder sections post 3rd
182 BCG revealed presence of ABCs and lymphoid aggregates, particularly prominent in female
183 bladder sections. Furthermore, higher proportion of splenic ABCs after B cell depletion is
184 indicative of accelerated expansion of ABCs potentially due to repeated weekly BCG treatment
185 with simultaneous BBN exposure (**Fig. 3I**). Indeed, removal of BBN exposure at the time of

186 treatment initiation reduced the frequency of splenic ABCs and CD21+ CD11c+ B cells in female
187 mice at one week after the 3rd BCG instillation (**Fig. S7)**. Overall, these findings suggested a
188 combination of carcinogen and BCG treatment induced expansion of ABCs that occurs at a higher
189 magnitude in females. Disease progression post repeated BCG instillations potentially reflects an
190 exhausted immune system.
191
192 **Sex chromosome associated factors influence B cell response following treatment with BCG**
193 The X chromosome harbors multiple B cell function associated genes such as *CD40L, CXCR3, TLR7,*
194 *IL9R, IL13RA1/2,* and *BTK*[41]. Furthermore, *TLR7* (known to escape X inactivation) and *IL13RA* are
195 also known to play key roles in the expansion of ABCs. We thus addressed the fundamental
196 question of whether sex-associated ABC expansion in BBN-exposed and BCG-treated mice is
197 influenced by gonadal hormones, sex chromosome complement, or a combination of both
198 factors. We employed 12-month-old aging FCG mice to investigate these interactions (**Fig. 4A**).
199 While no significant differences in the total splenic B cells (B220+CD19+) were observed between
200 the four genotypes; XXF (chromosomal and gonadal females), XYF (gonadal female), XXM
201 (chromosomal and gonadal males) and XYM (gonadal males) of the FCG mice (**Fig. S2C**), the XXF
202 mice exhibited significantly higher ABCs compared to all other genotypes (**Fig. 4B**). We then
203 investigated the sex associated expansion of ABCs in BBN-exposed BCG-treated FCG mice. Splenic
204 ABCs significantly decreased post 3rd BCG dose in the XXF mice compared to the BBN exposed
205 untreated, and saline groups (**Fig. 4B and Suppl. Table S8**). This shift was accompanied by a
206 simultaneous increase in the bone marrow frequency of ABCs at this time point, with a
207 significantly higher increase in XXF mice compared to the XYF, XYM, and XXM mice (**Fig. 4C**). The
208 BBN and BCG associated significant shifts were not observed within any other genotype of the
209 FCG mice indicating that ABC expansion is a plausible combined effect of both X chromosome
210 associated and hormonal factors. Histopathological evaluation revealed the presence of a higher
211 density of lymphoid aggregates in the bladder lamina propria of XXF mice at this time point
212 compared to XYF mice (**Fig. 4D)**. Similarly, H&E staining and mIF revealed an overall higher
213 immune cell infiltration in the bladders of XXM mice compared to the XYM mice (**Fig 4D and Fig.**

214 **S2D**). These findings confirmed a biological sex and age-associated expansion of ABCs in response
215 to BCG treatment.
216
217 To further confirm the response to ABC phenotype inducing stimuli, we treated splenic total B
218 cells (**Fig. 5A and 5B)**, isolated from BBN exposed 12-month-old female and male mice, to the
219 known ABC inducing cytokines, IFN-γ and IL-21 in the presence or absence of BCG. A significant
220 increase in the frequency of ABCs (CD21-CD11c+) in IL-21 treated B cells isolated from female
221 mice was confirmed *via* multiparametric flow cytometry at 18 hours post-treatment (**Fig. 5C; Fig.**
222 **S4B)**. Notably, B cells isolated from male mice did not show a similar increase in response to IL-
223 21 treatment (**Fig. 5C)**. However, CD11c+ B cells from male mice exhibited higher proportion of
224 CD21low/+ cells compared to the female mice (**Fig. S4C and S4D)**. The higher expression of CD21
225 in B cells isolated from male mice potentially suggests a delayed expansion of ABCs following
226 treatment with different ABC phenotype-inducing stimuli. Furthermore, stimulation with a TLR7
227 agonist (Imiquimod) significantly increased differentiation of splenic B cells, from both female
228 and male mice to ABCs (**Fig. S4E**). Gene expression analysis, using quantitative real time (qRT)-
229 PCR, revealed significant alterations in the expression of ABC associated genes *Fcrl5, Tbx21, and*
230 *Itgax* at 6 hours post-stimulation (**Fig. 5D-5F).** Treatment of splenic B cells from male mice with
231 IL-21 alone led to a significant increase in the expression *of Itgax* (**Fig. 5D**), indicative of higher
232 ABC differentiation. BCG infection elevated *Itgax* expression in B cells from female mice only
233 when added in combination with IFN-γ (**Fig. 5D**). Treatment with IFN-γ alone led to similar
234 increase in expression of *Tbx21*, only in B cells from females (**Fig. 5E**). However, in the presence
235 of both BCG and IFN-γ, increase in *Tbx21* expression was similar in B cells from both females and
236 males (**Fig. 5E**). In contrast, the combination of BCG infection with IL-21 and IFN-γ treatment
237 enhanced *Fcrl5* expression in male splenic B cells (**Fig.5F**). These findings indicate that BCG
238 infection drives a higher differentiation of ABCs in B cells isolated from female mice. Similarly,
239 multiplex cytokine analysis revealed significantly higher levels of GM-CSF, IL-10, IL-6, TNF-α, and
240 MCP-1 in the supernatants collected at 18 hours post-treatment of B cells from female mice
241 compared to those from males (**Fig. 5G-5K**). Internalization of BCG by B cells was confirmed *via*
242 immunofluorescence assay using an anti-LAM antibody (**Fig. S4F**). These findings underscore the

243 significance of considering sex-specific responses in B cell differentiation to ABCs following
244 treatment with IFN-γ and IL-21 in the presence or absence of BCG bacteria.
245
246 **B cell depletion during BCG treatment leads to enhanced recovery of the urothelium**
247
248 Our findings showing ABC expansion during disease progression prompted us to further
249 investigate whether B cell depletion alters the response to BCG immunotherapy in mice with
250 chronic exposure to BBN carcinogen. We found that depletion of B cells prior to and during BCG
251 treatment led to the return of urothelium to its benign morphological state in female mice (**Fig.**
252 **6A**). B cell depletion also led to reduced inflammation in the lamina propria of female mice (**Fig.**
253 **6A**) compared to male mice (**Fig. 6C**). In contrast, bladders from BCG-treated B cell intact female
254 (**Fig. 6B)** and male (**Fig. 6D)** mice showed dysplasia and focal CIS like changes at 1 week following
255 completion of treatment with 3 doses of BCG. TLS formation was rare or absent in the BCG + B-
256 cell-depleted mice (**Fig. 6E**) compared to B cell intact female mice (**Fig. 6F**). Exposure to BBN
257 carcinogen was maintained throughout the course of BCG treatment and B cell depletion to
258 mimic smoking behavior during BCG treatment. Indeed, removal of the BBN carcinogen at the
259 time of BCG treatment initiation in combination with B cell depletion revealed decreased invasion
260 into the sub-mucosal region (**Fig. S3C**).
261 Given the pronounced effect of depletion, specifically on the urothelium of female mice, we
262 examined the profiles of genes involved in immune cell recruitment and TLS formation using a
263 custom NanoString gene panel. The BCG-treated B cell-depleted group demonstrated an
264 increased expression of genes associated with an active effector immune state and antigen
265 processing**,** such as *Cd8A, Cxcl10, Cxcl9, H2Eb1, H2D1, H2K1, Stat1 and Batf3* (**Fig. 5G; Fig. S5)**.
266 On the other hand, bladders from mice that underwent repeated BCG treatment without B cell
267 depletion showed increased expression of genes associated with the expansion of ABCs and TLS
268 formation, such as *Tnf, Il6, Il17A, Cxcl13, Cd80, Cxcr4, Cxcr5, Cxcr1, Il1b, Ilr1, Tlr4, E2-2, Cd39, and*
269 *Tmem173* (**Fig 5G; Fig. S5**). These findings suggest that repeated weekly instillations of BCG lead
270 to the systemic expansion and trafficking of ABCs to the bladder microenvironment accompanied
271 by TLS formation. A combination effect of BBN carcinogen and BCG treatment induced sustained

272 inflammation may cause systemic expansion of exhausted immune cells during the contraction
273 phase thus augmenting disease progression.
274
275 **B cell depletion during BCG treatment alters the frequencies of helper and cytotoxic T cell**
276 **subsets**
277
278 Given that BCG primarily induces T helper type 1 (Th1) responses *via* activation of CD4+ T helper
279 cells, we explored the influence of B cell depletion on the profiles of T cell subsets and whether
280 this occurs in a sex differential manner. We did not observe any significant sex differences in
281 splenic total CD3+ T cell frequency at both early and late (post 3rd BCG) time points (**Fig. 7A and**
282 **7B**). Interestingly, the frequency of total CD3+ T cells in the bone marrow was significantly higher
283 in female mice post 3rd BCG compared to male mice (**Fig. 7B**). Notably, in the B cell depleted
284 group there was a significant increase in total splenic T cell frequency compared to the B cell
285 intact group in both sexes at this time point (**Fig. 7B**). Splenic immune profiles of saline treated
286 mice reflected catheterization induced sterile inflammation (data not shown), an effect that is
287 well established in both humans and mice[42,43]. A BCG specific immune response was revealed by
288 the changes in the urothelium (**Fig. S5A**) and the T cell profiles in the bone marrow (**Fig. 7B**) where
289 a significant increase in CD3+ T cell proportions was seen only in the female mice that received 3
290 doses of BCG with or without B cell depletion**.** A decline in splenic CD4+ T helper cells and CD8+
291 T cells following all 3 BCG instillations indicated potential recruitment to the bladder (**Fig. 7C -**
292 **7E**). Presence of high CD8+ T cells was confirmed by mIF of bladders collected at the same time
293 point (**Fig. S5A**). Overall, these findings confirm that in response to the administration of BCG *via*
294 intravesical (mucosal) route, the host elicits BCG specific T helper cell associated response that
295 augments a cancer cell specific cytotoxic immune response.
296
297 **B cell depletion during BCG treatment alters systemic and bladder infiltrating myeloid cell**
298 **functional states**
299

300 Bladder resident and recruited populations of myeloid cells are key to BCG response. In this study
301 we observed that BCG treatment led to significant alterations in the profiles of CD11b+ myeloid
302 cells in the spleen and bone marrow of both female and male mice. Overall, female mice depicted
303 a higher proportion of myeloid cells in the spleen compared to males. A small but significant
304 increase in splenic total CD11b+ myeloid cells, at 1 week post 1st BCG dose, was only observed in
305 the female mice compared to the male mice (**Fig. 8A and 8B).** Following completion of treatment
306 with all 3 doses of BCG, in both female and male mice, there was a significant decline in bone
307 marrow CD11b+ cells in contrast to mice undergoing B cell depletion during BCG (**Fig. 8B**). A
308 significant increase in splenic PD-L1 immune checkpoint expressing myeloid cells was observed
309 only in female mice following the 1st BCG dose (**Fig. 8C**). The proportion of PD-L1 expressing
310 myeloid cells was significantly higher following the 3rd BCG dose in the spleen and bone marrow
311 of both female and male mice that underwent B cell depletion during BCG treatment (**Fig. 8C and**
312 **8D)**. This was also confirmed by spatial immune profiling of bladders from the same mice where
313 increased infiltration of macrophages was observed (**Fig. 8E-8G).** Spatial immune profiling of
314 bladders revealed that the BCG + isotype treated female mice had increased infiltration of PD-
315 L1+ cells than the B cell-depleted group (**Fig. 8E-8G**). These findings suggest that the combination
316 of BBN exposure and repeated weekly BCG treatment induces sustained local inflammation,
317 which could potentially accelerate the exhaustion of systemic and bladder local antigen-
318 presenting cells (APCs).
319
320 **B cell depletion during BCG treatment of BBN exposed mice leads to elevated levels of**
321 **plasma Th1 and Th2 proinflammatory cytokines and antibodies in female mice**
322
323 Multiplex cytokine profiling of plasma collected following the completion of 3 doses of BCG
324 revealed significant differences in pro-inflammatory and immune cell activating cytokines key to
325 mediating Th1 and Th2 responses. In female mice undergoing B cell depletion during BCG
326 treatment, plasma levels of the Th1 cytokines; IL-2, IFN-γ, GM-CSF, MIP-1α and MIP-1β were
327 significantly higher compared to mice that did not undergo B cell depletion during BCG
328 treatment. Similarly, significantly increased Th2 cytokines such as IL-9 and IL-13 were observed

329 in mice subjected to B cell depletion during BCG treatment (**Fig. 9**). Healthy female mice displayed
330 higher plasma levels of IgM, IgG2a and IgG2b, compared to the age-matched male mice (**Fig.**
331 **S10B, S10C and S10D**). However, the levels of IgG2a declined at 7-week post BBN and 1 week
332 post 3rd BCG in female mice **(Fig. S10C**). Notably, in the female mice, the levels of IgG2b increased
333 from their pre-BCG levels reaching up to similar levels to those in age matched healthy controls,
334 despite the depletion of B cells during BCG treatment (**Fig. S10D**). In contrast, IgG2b levels
335 decreased significantly in B cell-depleted male mice (**Fig. S10D**). These findings suggest a critical
336 role of B cell subsets in inhibiting Th1 and Th2 responses induced by repeated mucosal BCG
337 administration in female mice.
338
339 **Discussion**
340
341 B cells and TLSs have emerged as biomarkers of favorable prognosis and response to
342 chemotherapy or immune checkpoint inhibitor therapy in some cancers including muscle-
343 invasive BC (MIBC)[44-46]. Recent reports also show that increased density and proximity of TA-TLSs
344 is associated with improved survival in patients with MIBC who are treated with adjuvant
345 chemotherapy or immune checkpoint inhibitors[47,48]. TA-TLSs are also associated with favorable
346 prognosis for patients with melanoma, renal, gastric, and lung cancers[49,50]. Contrary to this, in
347 colorectal, breast and hepatocellular carcinoma[51], a negative relationship between TA-TLSs and
348 patient outcomes has been demonstrated[52,53]. Similar to these and our previously reported
349 findings from pre-treatment tumors of patients with NMIBC and MIBC, findings from the current
350 study suggest their negative association with response to BCG[12]. This association may primarily
351 be attributed to the difference in local immunomodulation and downstream responses induced
352 by live BCG bacteria compared to systemically administered immune checkpoint inhibitors or
353 cytotoxic chemotherapy. The discrepancy also highlights the fact that the relationship between
354 TA-TLSs and cancer patient outcome depends on several parameters, including functional states
355 of immune cells within TLSs, persistence of carcinogen, treatment type, age/sex and disease
356 stage. While we observed high expression of immune cell exhaustion associated proteins in
357 chronically evolved pre-BCG TA-TLSs, it is plausible that the induction of acute TLSs post-BCG
358 would be associated with positive clinical outcomes given the ability of BCG to induce the

359 formation of granulomas[54]. However, this association may be reversed depending on the
360 persistence of carcinogen and recruitment of exhausted immune cell populations, from the
361 systemic circulation following repeated exposure to live BCG bacteria (as observed in our *in vivo*
362 studies).
363
364 TLSs may also play a pathological role by promoting auto-antibody production and harboring
365 immunosuppressive and dysfunctional immune cell populations due to sustained local
366 inflammation[55]. Indeed, previous reports in NMIBC showed significantly increased levels of
367 circulating IgG antibodies in patients exhibiting early recurrence post BCG[56]. This duality helps to
368 explain our findings as to why TLSs have been strongly associated with both positive and negative
369 outcomes in different cancer types. In this study, mIF based characterization of TLSs did not
370 reveal any significant differences in the density of TLSs in tumors from patients who subsequently
371 responded, compared to those who exhibited early recurrence post BCG. However, the location
372 and maturity of TLSs and proximity to tumor epithelium/invasive margin was indicative of an
373 aggressive tumor behavior accompanied with an exhausted local immune response.
374 Nevertheless, our findings from a cohort of 28 patients (89% male patients) provide novel insights
375 into TLS biology and emphasize the need for further validations in large independent cohorts.
376
377 BCG immunotherapy in NMIBC is unique with respect to its mucosal route of administration and
378 dosing schedule that requires repeated intravesical instillations at weekly intervals. Such
379 repeated exposure to BCG antigens, specifically during the induction phase, may cause an
380 expansion of exhausted immune cell populations in the effector memory phase. Such an
381 expansion may occur specifically in BCG unresponsive patients with a history of chronic or
382 persistent carcinogen exposure, smokers, patients with autoimmune conditions or female
383 patients with a history of recurrent urinary tract infections. The recent report by Strandgaard and
384 colleagues[57] demonstrated T cell exhaustion as a major factor underlying BCG failure. It is
385 plausible that in some patients, such repeated BCG induced immune activation will also lead to
386 increase in exhausted memory B cells and their recruitment to the bladder microenvironment
387 leading to less effective anti-tumor immune responses. This effect will be more pronounced in

388 older patients or those who exhibit higher pre-BCG intra-tumoral density of B cells within TA-
389 TLSs, reflective of their age-related/chronic carcinogen exposure induced profiles. It is tempting
390 to speculate that analogous to this T-bet transcription factor associated fate in both T and B cells,
391 expansion of ABCs (during the effector memory phase) may result from repeated encounter with
392 BCG bacteria in the induction phase, specifically, in unresponsive patients. This effect may
393 potentially also be more pronounced in female patients who generally experience early
394 recurrence and progression. Indeed, our previous report and unpublished findings from an on-
395 going study suggest that both female and male patients with high pre-treatment intra-tumoral B
396 cell density also experience early recurrence post BCG[12].
397
398 Patient age is an independent risk factor associated with poor response to BCG immunotherapy
399 in NMIBC[58]. Immunosenescence associated B cell alterations, governed by hormonal and sex
400 chromosome associated factors, accompany aging in a sex differential manner[23]. Indeed, immune
401 profiling of healthy aging mice confirmed the higher frequency of ABCs in females compared to
402 their male counterparts. Most importantly, using the FCG mouse model, we clearly established
403 that such sex differences in BCG induced systemic immune profiles as well as bladder associated
404 lymphoid aggregate formation, are influenced by both gonadal hormones and X chromosome
405 linked factors. Based on our *in vivo* findings, we reason that BCG internalized by ABCs in the
406 bladder microenvironment/TLSs, activates the TLR9 pathway following the binding of bacterial
407 CpG DNA[35]. Such an amplified TLR9 response could lead to the production of immunosuppressive
408 IL-10, which may further inhibit anti-tumor T cell responses and polarize macrophages to M2-like
409 suppressive states. *In vitro* infection of B cells using BCG bacteria confirmed such an increase in
410 IL-10. Further, significant decrease in PD-L1 expression in bladders B cell-depleted BCG-treated
411 female mice reflects a favorable anti-tumor immune response.
412
413 Validation to the central role of B cells, in mediating responses to BCG, is reinforced by
414 noteworthy observations from our study. Notably, the depletion of B cells during BCG treatment
415 reduced inflammation in the urothelium and helped accelerate its recovery despite the presence
416 of carcinogen specifically in female mice. Additionally, the recovery of urothelium was
417 accompanied by significant increases in circulating levels of the cytokines such as IL-2, IFN-γ, IL-9

418 and IL-13 that favor a Th1 and Th2 response. These cytokines play crucial roles in enhancing the
419 immune system's ability to fight against cancer cells and facilitate the resolution of inflammation.
420 Furthermore, increased expression of *Cd8A, Cxcl10, Cxcl9, H2-Eb1, H2-d1,* and *Batf3* was
421 observed in bladders from mice undergoing B cell depletion during BCG treatment. A higher
422 expression of *Cd8A* in the depleted group indicated a higher T cell density, which is also supported
423 by our findings from mIF of whole bladder sections from the depleted group. Conversely, the
424 upregulation of *Batf3* suggests either increased DCs or the suppression of T regulatory cells, in
425 the depleted group. On the other hand, the BCG treated group exhibited higher expression of
426 genes linked to ABC expansion and TLS formation, such as *Tnf, Il6, Il17, Cxcl13, Cxcr4, Cxcr5, Cxcr1,*
427 *Cd80* and *Il1B.* These findings align with our hypothesis that ABC expansion and recruitment
428 following repeated BCG treatment could contribute to an exhaustive bladder microenvironment,
429 potentially leading to early disease recurrence. These gene expression patterns further
430 corroborate the differential immune responses observed between the two treatment groups,
431 emphasizing the pivotal role of B cells in shaping the response to BCG immunotherapy. Despite
432 the depletion of B cells, comparable levels of IgM, IgG2a, and IgG2b between the healthy control
433 and B cell-depleted female mice is suggestive of a memory B cell response triggered by BCG
434 infection given the enhanced rejuvenation of lymphopoiesis in females. It is known that the
435 cytokine IL-21 (inhibits CD8+ T cell cytolytic function), which governs ABC expansion, plays
436 opposite roles compared to those of IL-2 (promotes cytotoxic function of CD8+ T cells)[59]. B cell
437 depletion prior to initiation of BCG treatment may thus ablate such IL-21 mediated suppression
438 of T cell function thus enhancing anti-tumor immunity especially in females or males with high
439 TA-TLSs.
440
441 Our study is not without limitations. We did not establish the precise *in vivo* cellular trafficking
442 associated events following BCG. However, our finding that CD3+CD8- T cells were significantly
443 expanded post 3rd BCG in both B cell depleted and non-depleted mice, suggests that BCG bacteria
444 travel to the bone marrow where further cellular priming and activation may occur. While
445 findings from this study demonstrate the critical role of B cells and ABCs in mediating response
446 to BCG, the mechanistic basis of how these cells suppress anti-tumor cytotoxic response remains
447 unclear and needs further investigation. Future investigations could also explore the BCG dose

448 related aspects of differential response to BCG in the context of sex related immune physiology.
449 It is established that B cell associated CD21 (complement receptor 2) binds to autoantigens or
450 immune complexes,[60] and also interacts with TLR9. Most importantly CD21/CR2 has been shown
451 to be critical for the internalization of BCG bacteria by B cells.[61] The role of the complement
452 cascade in mediating response to BCG in NMIBC has not been explored and needs further
453 investigation.
454
455 Overall, this study not only advances the current understanding of the BCG mode of action in the
456 context of bladder mucosal immunity but also provides the first evidence for a critical role of B
457 cell exhaustion, reflected by higher pre-BCG TA-TLSs and expansion of ABCs, in disease
458 progression and treatment response. While mouse models do not reflect the disease complexity
459 observed in human scenarios, our study considers aging aspects of the immune system, unique
460 aspects of the mucosal immune responses and sex differences *via* the inclusion of mice from both
461 sexes and the FCG mice. Taken together, these novel findings based on human specimens and *in*
462 *vivo* studies, partially explain the poor outcomes in female patients and in male patients with
463 high intra-tumoral B cells and TA-TLSs in their pre-treatment tumors. Therapeutic targeting of
464 ABC associated markers in combination with optimal sequencing of PD-L1 immune checkpoint
465 blockade could be a novel approach for treatment of patients identified early based on their
466 systemic and bladder associated immune profiles.
467
468
469 **Materials and Methods**
470
471 **Human NMIBC tumor specimens**
472
473 All studies involving the use of patient materials were approved by the Human Ethics Review
474 Board at Queen's University. The cohort comprised of 28 patients (25 males and 3 females) with
475 NMIBC who underwent TURBT surgery at Kingston Health Sciences Centre (KHSC) between
476 March 2016 and November 2017. Formalin-fixed paraffin-embedded (FFPE) tumor specimens
477 were retrieved from the Department of Pathology at Queen's University. Patient clinical details

478 were retrieved *via* electronic chart review (DJ). All patients in the cohort received adequate
479 induction of BCG immunotherapy (>5 out of 6 doses) following index TURBT surgery. Response
480 to BCG was defined as the time from each patient's earliest TURBT resection to next malignant
481 diagnosis. Operative notes were reviewed to exclude re-resections as recurrences. Patients who
482 had recurrence-free survival greater than 2 years were classified as BCG-responders (n=15).
483 Patients who had recurrence-free survival less than 1 year were classified as BCG-non-responders
484 (n=13).
485
486 **Multiplex immunofluorescence on whole tumor sections**
487
488 We employed mIF to characterize the organization and maturity of TLSs found in tumors from
489 NMIBC patients. Using our selected archival FFPE samples, triplicate 5 µm sections were cut and
490 mounted at Queen's Laboratory for Molecular Pathology (QLMP). One section per sample was
491 subjected to H&E staining. Stained sections were subjected to high-resolution scanning (Olympus
492 VS120 Scanner) and the scans were uploaded for viewing on the web-based HALO® image hosting
493 service. Immune cell aggregates, mature TLSs, and other areas of interest were electronically
494 annotated and reviewed for accuracy by a trained pathologist (MX).
495
496 An unstained section from each of the samples was stained *via* automated mIF staining at the
497 Molecular and Cellular Immunology Core facility (Deeley Research Centre; Vancouver, British
498 Columbia, Canada). Samples were stained with fluorophore-conjugated primary antibodies
499 against cell surface proteins to identify B cells, T cells, DCs and high endothelial venules (**Suppl.
500 Table S4**). Stained sections were scanned using the Vectra multispectral imaging system and
501 viewed using PhenoChart 1.1.0 Software (Akoya BioSciences®; Marlborough, Massachusetts,
502 USA). Aggregates/TLSs were classified into primary (immature) or secondary (mature) follicle as
503 previously reported.[19]
504
505 **Digital spatial profiling of immune pathway proteins using NanoString's GeoMx platform**
506

507 We employed NanoString GeoMx™ DSP technology to spatially characterize the protein
508 expression profiles in TLSs and epithelial regions within a subset of NMIBC tumors (6 responders
509 and 6 non-responders). This unique, high-throughput multiplexed technique uses indexing
510 oligonucleotides to quantify the spatially resolved abundance of protein or RNA from FFPE tissue
511 sections. Unstained fresh-cut 5 µm sections from the selected samples were processed on the
512 NanoString GeoMx DSP platform at the Imaging Centre (University of Minnesota, USA). Slide
513 processing was performed as per the manufacturer's instructions using DNA stain (SYTO 13), pan-
514 Cytokeratin (epithelium), CD45 (immune cells) and CD20 (B cells) antibodies to guide selection of
515 regions of interest. The abundance and localization of 49 immune proteins of interest (Immune
516 Cell Profiling Core, plus the Immuno-Oncology, Drug Target Module, Immune Activation Status
517 Module, and the Immune Cell Typing Module; see **Suppl. Table S2**) was measured. Quality control
518 was performed as per the manufacturer's instructions and External RNA Controls Consortium in
519 DSP suite (nCounter™ platform) prior to further analysis. Details of the DSP methodology and
520 analysis are provided in the Supplementary data.
521
522 ***In vivo* studies**
523 **Animal models**
524
525 All murine experiments were in accordance with the guidelines provided by Queen's University
526 Animal Care Committee and approved in an animal research protocol. The B6.Cg-Tg(Sry)2Ei
527 Srydl1Rlb/ArnoJ mice were kindly provided by Dr. Manu Rangachari (University of Laval) and also
528 purchased from the Jackson laboratory (stock number 010905, RRID:SCR_002187). Breeding of
529 the FCG mice was conducted at the Queen's animal care facility to derive the four genotypes
530 (gonadally female mice and male mice with XX and XY chromosomal complement each). The FCG
531 transgenic mouse model (on a C57BL/6 background) allows for the generation of sex-reversed XX
532 males and XY females by breeding mice with a loss-of-function mutation in the Y chromosome-
533 linked testes-determining *Sry* gene with transgenic mice carrying an *Sry* rescue transgene on an
534 autosome (**Fig. 4A**)[62]. This model permits determination of independent effects of gonadal and
535 sex chromosome-specific features on bladder cancer progression associated immunologic

536 profiles. Mice were aged for 12 months at the facility. Wild type C57BL/6 female and male mice
537 (12 months old) were purchased from Charles River Laboratory (Montreal, QC, Canada). All mice
538 were fed sterilized conventional diet and water and maintained under specific pathogen-free
539 environment.
540
541 **BBN carcinogen exposure and depletion of B cells**
542
543 Female and male C57BL/6 mice (12 months old) and FCG mice (12 months old) were administered
544 0.05% BBN (Cat# B0938, TCI America, OR, USA) *ad libitum* in drinking water (protected from light)
545 once a week for 7-12 weeks as previously described.[18] Our previous findings have demonstrated
546 the formation of lymphocyte aggregates, within the lamina propria of bladder, initiating at week
547 4 post BBN exposure as a result of BBN induced DNA damage[40]. To determine the influence of B
548 cells on disease progression, we initiated B cell depletion starting week 3 post BBN exposure.
549 Briefly, a cocktail of monoclonal antibodies (**Suppl. Table S3**) at 150 µg/mouse: rat anti-mouse
550 CD19, rat anti-mouse B220 and mouse anti-mouse CD22 was injected *via* intraperitoneal (I.P)
551 injection, as described previously[39]. After 48 hours, mice were injected with mouse anti-rat κ
552 secondary antibody at 150 µg/mouse. To maintain the depletion of B cells *in vivo*, mice were
553 injected with anti-CD20 antibody. B cell depletion cocktail injections were repeated 3 times every
554 10 days to ensure the complete depletion of systemic B cells, further confirmed with flow
555 cytometry results post last injection. To determine the effect of B cell depletion on response to
556 BCG in BBN exposed mice, depletion protocol was initiated 1 week prior to 1st BCG instillation
557 followed by weekly anti-CD20 antibody injections for 3 weeks during BCG treatment. Isotype
558 controls for each antibody (**Suppl. Table S3**) mentioned above were also used.
559
560 **Intravesical BCG in BBN exposed mice**
561 Lyophilized TICE strain of BCG (Merck, Canada) was obtained from the pharmacy at KHSC. Each
562 50 mg vial contained 1 - 8 x 10^8 colony forming units (CFU) of BCG, as tested by the manufacturer.
563 BCG was resuspended in sterile saline for all experiments. At 7 weeks post BBN exposure, mice
564 were subjected to intravesical treatment with 3 weekly instillations of BCG (1mg/mouse in 50 µl

565 of saline). BCG was delivered *via* transurethral catheterization with a 24-gauge catheter (3/4",
566 Cat# 4053, Jelco, Minneapolis, USA) for female mice and PE-10 tubing in male mice under
567 isoflurane anaesthesia. Urethral VASCU-STATT Midi clamps (Cat# 1001-501, Scanlan, Canada)
568 were placed to hold BCG within the bladder for 1 hour. Whole bladders were collected from all
569 treatment groups post 1st (8 weeks post BBN exposure) and 3rd BCG (10 weeks post BBN
570 exposure) instillation, post 1st anti-CD20 treatment after 1st BCG instillation (8 weeks post BBN
571 exposure) and post 3rd anti-CD20 treatment after 3rd BCG (10 weeks post BBN exposure)
572 instillation (**Fig. 3A**) and fixed in 4% paraformaldehyde for histopathological evaluation and
573 spatial immune profiling *via* mIF. Single cell suspensions from bone marrow and spleen were
574 subjected to profiling using multispectral flow cytometry. Blood was collected from the
575 submandibular vein for plasma cytokine profiling.
576
577
578 **Local and systemic immune profiling**
579 Whole bladders collected from all treatment groups, at treatment time points as indicated in **Fig.**
580 **3A**, were sagittaly cut into two halves, fixed in 10% formalin and paraffin-embedded for H&E
581 staining as described in above section. The urothelial changes in mice were classified as follows:
582 reactive atypia, dysplasia, carcinoma in situ (CIS), early invasion and invasion. 5 µm unstained
583 FFPE sections were subjected to spatial immune profiling using mIF staining to determine the
584 infiltration patterns of selected immune markers. Antibodies to identify CD11b+ myeloid cells,
585 CD3+ total T cells, CD8+ cytotoxic T cells, Pax5+ B cells, CD19+ CD21- CD11c+ atypical B cells, PD-
586 L1+ cells (**Suppl. Table S4**) were used in mIF staining at the Molecular and Cellular Immunology
587 Core (MCIC) facility, BC Cancer Agency as per previously reported methods.[18] Multiplex IF stained
588 images were acquired using the Vectra 3 multichannel imaging system. Images were then
589 imported to Phenochart (11.0, Akoya Biosciences) and Inform Viewer (2.5.0, Akoya Biosciences)
590 software for annotation followed by capturing at high magnification. The Inform Viewer was used
591 to visualize a detailed composite image of each section with the flexibility of spectral separation
592 of all the fluorophores from each panel. StarDist (https://github.com/stardist/stardist), a deep
593 learning tool extension available in the QuPath software (https://qupath.github.io, v0.40) was

594 used to further analyze the expression of markers within a region of interest (ROI)[63]. Positive
595 staining thresholds were manually defined for each marker following confirmation using the DAPI
596 nuclear stain channel. Immune cell infiltration was evaluated in 10 random annotated ROI
597 adjacent to the basal layer of the urothelium in the bladders for each treatment group.
598 Composite object classifier tool was used to identify co-expression of markers. Measurements
599 were calculated per mm^2 and exported to GraphPad Prism (v9.5.1, California, USA) to analyze
600 differences between sexes and treatment groups.
601
602 Single cell suspensions from spleens harvested were prepared by mechanical dissociation. Bone
603 marrow was aspirated with RPMI-1640 media (Wisent Bioproducts, ON, Canada) using a 26-
604 gauge needle and passing it through a 40 µm cell strainer followed by red blood cell (RBC) lysis.
605 Details of further processing and multiparametric flow cytometry (Cytoflex-S; Beckman, USA) are
606 provided in the **Supplementary methods** section.
607
608 **Gene expression profiling of bladder using NanoString nCounter gene expression platform**
609
610 Gene expression profiling was performed on total RNA isolated from fresh frozen whole bladders
611 using a custom designed nCounter gene panel (**Suppl. Table S7)** which included genes associated
612 with immune function, various cancer-related chemokines and cytokines, and housekeeping
613 genes (NanoString Technologies, Washington, USA). Because of the significant changes observed
614 in urothelium of female bladders following B cell depletion during BCG treatment, this analysis
615 was only performed in bladders from female mice. Total RNA from fresh frozen bladders (as
616 indicated) was isolated using the RNeasy Mini Kit (Cat. #74004, Qiagen, Hilden, Germany) as
617 per the manufacturer's instructions. The purity and concentration of isolated RNA was
618 assessed using the NanoDrop ND-100 spectrophotometer (NanoDrop Technologies, DE,
619 USA). Total RNA (150 ng) was used as a template for digital multiplexed profiling at Ontario
620 Institute for Cancer Research as per previously established protocols. The nSolver software
621 (NanoString Technologies, Washington, USA) was used to normalize the raw nCounter
622 NanoString counts using built-in positive controls. Normalization was performed using

623 housekeeping genes and overall assay efficiency was calculated using geometric mean of
624 each control. Normalized nCounter gene counts between different treatment groups was
625 further analysed in GraphPad Prism.
626
627 **Plasma cytokine profiling and immunoglobulin isotyping**
628
629 Female and male mice from each treatment group (n = 4-5 mice per group) were subjected to
630 blood collection from the submandibular (facial) vein. Separated plasma was aliquoted as per the
631 requirements for multiplex cytokine analysis and stored at -80°C until further profiling. Plasma
632 was diluted using PBS (1:1) and subjected to multiplex cytokine analysis using the commercially
633 available 32-Plex Mouse Cytokine Discovery Array (MD-31; Eve Technologies, AB, Canada).
634
635 Plasma Ig were analysed using the LEGENDplex Mouse Immunoglobulin Isotyping panel (6-plex)
636 by flow cytometry (Cat #740493, BioLegend, CA, USA). Plasma sample and standards was
637 prepared using assay buffer as per the manufacturer's instruction. Data was analysed using the
638 cloud-specific LEGENDplex Data Analysis Software Suite Qognit (v.2023.02.15, CA, USA).
639 Statistically significant differences in the levels of Ig isotypes between the groups were
640 determined using GraphPad Prism.
641
642 ***In vitro* studies**
643
644 **Cell culture**
645
646 Splenic B cells were isolated from 12-month-old female and male mice (n=3-4/group) after 7
647 weeks of BBN exposure using EasySep Mouse Pan B cell negative isolation kit (Cat# 19844,
648 StemCell technologies, BC, Canada). The purity and viability of enriched B cells was >90% as
649 assessed by anti-B220 and anti-CD19 mAb staining using flow cytometry (**Fig. 5A; Fig. S5A).** B cells
650 were resuspended in a base B cell culture media comprising of RPMI media supplemented with
651 L-glutamine, 10% FBS, 1% Penicillin/Streptomycin, 1X Sodium Pyruvate, 50 µM 2-

652 mercaptoethanol, 1X Nonessential amino acid and 10mM HEPES. 1.5 x 10^6 cells/ml were seeded
653 in a 96 well plate and treated with IFN-γ (20ng/ml, Cat#315-05, Peprotech, NJ, USA), IL-21 (20
654 ng/ml, Cat# 210-21, Peprotech, NJ, USA) and TLR7 agonist – Imiquimod (R837) (2.5µM, Cat# tlrl-
655 imqs, Invivogen, CA, USA) for 6 and 18 hours at 37°C and 5% CO_2. Cells were also infected with
656 BCG TICE (Merck, Canada) along with IFN-γ and IL-21 to compare the expansion of ABCs.
657 Lyophilized BCG was reconstituted in B cell culture media at a concentration of 1 mg/ml, resulting
658 in approximately 0.2 – 1.6 x 10^7 CFU per ml. Following an 18-hour treatment, the supernatant
659 was collected, and cells were subjected to flow cytometric analysis using the ABC panel
660 (**Supplementary methods**).
661
662 **Quantitative real-time PCR**
663
664 After 6 hrs of *in vitro* treatment, total RNA was extracted from the B cells using the RNeasy Mini
665 Kit (Cat. #74004, QIAGEN, Germany) as per the manufacturer's instruction. The quality and
666 concentration of the RNA was assessed by the NanoDrop ND-100 spectrophotometer
667 (NanoDrop Technologies, DE, USA). 150 ng of total RNA per sample was used to synthesize
668 cDNA using LunaScript RT SuperMix kit (Cat# E3010L, NewEngland BioLabs, MA, USA) in a
669 20 µl reaction volume. Quantitative real-time PCR was performed using ViiA 7 Real-Time
670 PCR System (Applied Biosystems, MA, USA). Briefly, the 20 µl reaction volume consisted of
671 10 µl of TaqMan Fast Advanced Master Mix (Cat# 4444556, Applied Biosystems, MA, USA),
672 2 µl of cDNA, 1 µl of TaqMan primers (**Suppl. Table S6)** and 7 µl of nuclease free water.
673 Relative gene expression was calculated using $2^{-\Delta\Delta Ct}$ method and *Ubc* as the housekeeping
674 gene.
675
676 **Multiplex cytokine profiling of culture supernatants**
677
678 Supernatants collected after 18 hours of treatment was aliquoted in separate tubes and stored
679 at -80°C until further profiling. Supernatant was subjected to multiplex cytokine analysis using

680 commercially available Mouse Cytokine Proinflammatory Focused 10-plex Discovery Array (MD-
681 F10; Eve Technologies, AB, Canada).
682
683 **Immunocytochemistry**
684 Splenic B cells, enriched *via* negative selection, were treated with IFN-γ, IL-21, TLR7, and BCG
685 infection for 6 hours and 18 hours. The treated cells were then transferred to cover slips pre-
686 coated with a 0.1% Poly-L-lysine solution (Cat# P8920, Millipore Sigma, MO, USA) and incubated
687 at 37°C with 5% CO_2 for 1 hour. Next, the cells were fixed with 4% paraformaldehyde (PFA) for
688 30 minutes at room temperature (RT) and blocked with 5% skim milk for 30–45 minutes at RT.
689 Subsequently, the cells were incubated with primary antibodies Anti-CD11c and Anti-LAM (**Suppl.**
690 **Table S5**) overnight at 4°C. The cells were then incubated with the corresponding secondary
691 antibodies (**Suppl. Table S5**) for 1 hour at RT. All intermediate washes were performed using PBS-
692 T (0.1% Tween 20) buffer. Finally, ProLong Gold Antifade Mountant with DNA stain DAPI (Cat#
693 P36941, Invitrogen, MA, USA) was used to prevent photobleaching, and the cells were
694 transferred onto slides. The slides were visualized using a Zeiss Axio Imager M2 epifluorescence
695 microscope (Zeiss, Germany).
696
697 **Statistical Analysis**
698
699 Statistical analysis was performed using GraphPad Prism. Results are expressed as mean ± SD.
700 Comparisons between two groups with one independent variable was performed using non-
701 parametric t-test (Mann-Whitney). Three or more groups with one independent variable were
702 analysed using one-way ANOVA with Tukey's post hoc test. Three or more groups with two or
703 more independent variable were analysed using two-way ANOVA with Tukey's multiple
704 comparison test. Statistical significance is indicated by *$p<0.05$, **$p<0.01$, ***$p<0.001$,
705 ****$p<0.001$, ns - not significant.
706
707 **Author contributions and acknowledgements**
708

709 MK conceptualized and designed the study. PY, SR, SC, GC and MK performed experiments
710 included in this study, analyzed data and contributed to manuscript writing and reviewing. IE
711 helped with BBN experiments. KS and JH analyzed the NanoString GeoMx DSP data. DJ helped
712 with chart review and identification of BCG responders and non-responders. MX helped with
713 reviewing histopathological features and retrieving the archival tumor tissue specimens. DRS and
714 DMB helped with clinical classifications of BCG treated patient specimens. EM and JM designed
715 the Nanostring nCounter panel in consultation with WK. All authors reviewed the manuscript.
716 This study was supported by research operating grants from Bladder Cancer Canada, Cancer
717 Research Society, Ontario Ministry of Research Innovation and Science: Early Researcher Award
718 and Canada Foundation for Innovation, to MK. We thank Lee Boudreau at QLMP for his assistance
719 with embedding of FFPE blocks, sectioning, and H&E staining. We thank Shakeel Virk at the QLMP
720 for his assistance with imaging and Halo software and Katy Milne at BC Cancer's Molecular and
721 Cellular Immunology Core (MCIC) for immunofluorescence staining of TMAs. Dr. Patricia Lima at
722 the Queen's Cardiopulmonary Unit helped with optimization of ABC panel and confocal
723 microscopy-based imaging of multiplex IF stained whole bladder sections. We thank Dr. Andrew
724 Winterborn and the staff at the Queen's animal care facility for all the support with animal
725 studies.

References

1 Lobo, N. *et al.* Epidemiology, Screening, and Prevention of Bladder Cancer. *Eur Urol Oncol* **5**, 628-639, doi:10.1016/j.euo.2022.10.003 (2022).

2 Koti, M. *et al.* Adaptive Immunity in Genitourinary Cancers. *Eur Urol Oncol*, doi:10.1016/j.euo.2023.03.002 (2023).

3 Saginala, K. *et al.* Epidemiology of Bladder Cancer. *Med Sci (Basel)* **8**, doi:10.3390/medsci8010015 (2020).

4 Richters, A., Leliveld, A. M., Goossens-Laan, C. A., Aben, K. K. H. & Ozdemir, B. C. Sex differences in treatment patterns for non-advanced muscle-invasive bladder cancer: a descriptive analysis of 3484 patients of the Netherlands Cancer Registry. *World J Urol* **40**, 2275-2281, doi:10.1007/s00345-022-04080-6 (2022).

5 Viswambaram, P. & Hayne, D. Gender discrepancies in bladder cancer: potential explanations. *Expert Rev Anticancer Ther* **20**, 841-849, doi:10.1080/14737140.2020.1813029 (2020).

6 Gul, Z. G., Liaw, C. W. & Mehrazin, R. Gender Differences in Incidence, Diagnosis, Treatments, and Outcomes in Clinically Localized Bladder and Renal Cancer. *Urology* **151**, 176-181, doi:10.1016/j.urology.2020.05.067 (2021).

7 Marks, P. *et al.* Female with bladder cancer: what and why is there a difference? *Transl Androl Urol* **5**, 668-682, doi:10.21037/tau.2016.03.22 (2016).

8 Bree, K. K. *et al.* All High-Grade Ta Tumors Should Be Classified as High Risk: Bacillus Calmette-Guerin Response in High-Grade Ta Tumors. *J Urol* **208**, 284-291, doi:10.1097/JU.0000000000002678 (2022).

9 Babjuk, M. *et al.* European Association of Urology Guidelines on Non-muscle-invasive Bladder Cancer (Ta, T1, and Carcinoma in Situ). *Eur Urol* **81**, 75-94, doi:10.1016/j.eururo.2021.08.010 (2022).

10 Roumiguie, M. *et al.* International Bladder Cancer Group Consensus Statement on Clinical Trial Design for Patients with Bacillus Calmette-Guerin-exposed High-risk Non-muscle-invasive Bladder Cancer. *Eur Urol*, doi:10.1016/j.eururo.2021.12.005 (2021).

11 Lobo, N. *et al.* Updated European Association of Urology (EAU) Prognostic Factor Risk Groups Overestimate the Risk of Progression in Patients with Non-muscle-invasive Bladder Cancer Treated with Bacillus Calmette-Guerin. *Eur Urol Oncol*, doi:10.1016/j.euo.2021.11.006 (2021).

12 Chenard, S. *et al.* Sexual Dimorphism in Outcomes of Non-muscle-invasive Bladder Cancer: A Role of CD163+ Macrophages, B cells, and PD-L1 Immune Checkpoint. *Eur Urol Open Sci* **29**, 50-58, doi:10.1016/j.euros.2021.05.002 (2021).

13 Schumacher, T. N. & Thommen, D. S. Tertiary lymphoid structures in cancer. *Science* **375**, eabf9419, doi:10.1126/science.abf9419 (2022).

14 Tam, A. *et al.* Sex differences in lymphoid follicles in COPD airways. *Respir Res* **21**, 46, doi:10.1186/s12931-020-1311-8 (2020).

15 Lu, K. *et al.* Identification of novel biomarkers in Hunner's interstitial cystitis using the CIBERSORT, an algorithm based on machine learning. *BMC Urol* **21**, 109, doi:10.1186/s12894-021-00875-8 (2021).

16 Akiyama, Y. *et al.* Autoimmunity to urothelial antigen causes bladder inflammation, pelvic pain, and voiding dysfunction: a novel animal model for Hunner-type interstitial cystitis. *Am J Physiol Renal Physiol* **320**, F174-F182, doi:10.1152/ajprenal.00290.2020 (2021).

17 Ligon, M. M. *et al.* Single cell and tissue-transcriptomic analysis of murine bladders reveals age- and TNFalpha-dependent but microbiota-independent tertiary lymphoid tissue formation. *Mucosal Immunol*, doi:10.1038/s41385-020-0290-x (2020).

18 Hamade, A. *et al.* Sex differences in the aging murine urinary bladder and influence on the tumor immune microenvironment of a carcinogen-induced model of bladder cancer. *Biol Sex Differ* **13**, 19, doi:10.1186/s13293-022-00428-0 (2022).
19 Koti, M. *et al.* Tertiary Lymphoid Structures Associate with Tumour Stage in Urothelial Bladder Cancer. *Bladder Cancer* **3**, 259-267, doi:10.3233/BLC-170120 (2017).
20 Moyron-Quiroz, J. E. *et al.* Role of inducible bronchus associated lymphoid tissue (iBALT) in respiratory immunity. *Nat Med* **10**, 927-934, doi:10.1038/nm1091 (2004).
21 Rangel-Moreno, J. *et al.* Omental milky spots develop in the absence of lymphoid tissue-inducer cells and support B and T cell responses to peritoneal antigens. *Immunity* **30**, 731-743, doi:10.1016/j.immuni.2009.03.014 (2009).
22 Robson, K. J. & Kitching, A. R. Tertiary lymphoid tissue in kidneys: understanding local immunity and inflammation. *Kidney Int* **98**, 280-283, doi:10.1016/j.kint.2020.04.026 (2020).
23 Marquez, E. J. *et al.* Sexual-dimorphism in human immune system aging. *Nat Commun* **11**, 751, doi:10.1038/s41467-020-14396-9 (2020).
24 Phalke, S. *et al.* Molecular mechanisms controlling age-associated B cells in autoimmunity. *Immunol Rev*, doi:10.1111/imr.13068 (2022).
25 Sachinidis, A., Xanthopoulos, K. & Garyfallos, A. Age-Associated B Cells (ABCs) in the Prognosis, Diagnosis and Therapy of Systemic Lupus Erythematosus (SLE). *Mediterr J Rheumatol* **31**, 311-318, doi:10.31138/mjr.31.3.311 (2020).
26 Hao, Y., O'Neill, P., Naradikian, M. S., Scholz, J. L. & Cancro, M. P. A B-cell subset uniquely responsive to innate stimuli accumulates in aged mice. *Blood* **118**, 1294-1304, doi:10.1182/blood-2011-01-330530 (2011).
27 Mouat, I. C. & Horwitz, M. S. Age-associated B cells in viral infection. *PLoS Pathog* **18**, e1010297, doi:10.1371/journal.ppat.1010297 (2022).
28 Rubtsov, A. V. *et al.* Toll-like receptor 7 (TLR7)-driven accumulation of a novel CD11c(+) B-cell population is important for the development of autoimmunity. *Blood* **118**, 1305-1315, doi:10.1182/blood-2011-01-331462 (2011).
29 Cancro, M. P. Age-Associated B Cells. *Annu Rev Immunol* **38**, 315-340, doi:10.1146/annurev-immunol-092419-031130 (2020).
30 Ratliff, M., Alter, S., Frasca, D., Blomberg, B. B. & Riley, R. L. In senescence, age-associated B cells secrete TNFalpha and inhibit survival of B-cell precursors. *Aging Cell* **12**, 303-311, doi:10.1111/acel.12055 (2013).
31 Riley, R. L., Khomtchouk, K. & Blomberg, B. B. Age-associated B cells (ABC) inhibit B lymphopoiesis and alter antibody repertoires in old age. *Cell Immunol* **321**, 61-67, doi:10.1016/j.cellimm.2017.04.008 (2017).
32 Zhang, W. *et al.* Excessive CD11c(+)Tbet(+) B cells promote aberrant TFH differentiation and affinity-based germinal center selection in lupus. *Proc Natl Acad Sci U S A* **116**, 18550-18560, doi:10.1073/pnas.1901340116 (2019).
33 Rakhmanov, M. *et al.* Circulating CD21low B cells in common variable immunodeficiency resemble tissue homing, innate-like B cells. *Proc Natl Acad Sci U S A* **106**, 13451-13456, doi:10.1073/pnas.0901984106 (2009).
34 Mouat, I. C., Goldberg, E. & Horwitz, M. S. Age-associated B cells in autoimmune diseases. *Cell Mol Life Sci* **79**, 402, doi:10.1007/s00018-022-04433-9 (2022).
35 Guerrier, T. *et al.* TLR9 expressed on plasma membrane acts as a negative regulator of human B cell response. *J Autoimmun* **51**, 23-29, doi:10.1016/j.jaut.2014.02.005 (2014).
36 Cornelie, S. *et al.* Direct evidence that toll-like receptor 9 (TLR9) functionally binds plasmid DNA by specific cytosine-phosphate-guanine motif recognition. *J Biol Chem* **279**, 15124-15129, doi:10.1074/jbc.M313406200 (2004).

820 37 Antonelli, A. C., Binyamin, A., Hohl, T. M., Glickman, M. S. & Redelman-Sidi, G. Bacterial
821 immunotherapy for cancer induces CD4-dependent tumor-specific immunity through tumor-
822 intrinsic interferon-γ signaling. *Proc Natl Acad Sci U S A* **117**, 18627-18637,
823 doi:10.1073/pnas.2004421117 (2020).
824 38 Bafica, A. *et al.* TLR9 regulates Th1 responses and cooperates with TLR2 in mediating optimal
825 resistance to Mycobacterium tuberculosis. *J Exp Med* **202**, 1715-1724,
826 doi:10.1084/jem.20051782 (2005).
827 39 Keren, Z. *et al.* B-cell depletion reactivates B lymphopoiesis in the BM and rejuvenates the B
828 lineage in aging. *Blood* **117**, 3104-3112, doi:10.1182/blood-2010-09-307983 (2011).
829 40 Toyoda, T. & Ogawa, K. Early detection of urinary bladder carcinogens in rats by
830 immunohistochemistry for gamma-H2AX: a review from analyses of 100 chemicals. *J Toxicol*
831 *Pathol* **35**, 283-298, doi:10.1293/tox.2022-0061 (2022).
832 41 Yu, B. *et al.* B cell-specific XIST complex enforces X-inactivation and restrains atypical B cells. *Cell*
833 **184**, 1790-1803 e1717, doi:10.1016/j.cell.2021.02.015 (2021).
834 42 Rousseau, M. *et al.* Bladder catheterization increases susceptibility to infection that can be
835 prevented by prophylactic antibiotic treatment. *JCI Insight* **1**, e88178,
836 doi:10.1172/jci.insight.88178 (2016).
837 43 Hazen, J. E., Di Venanzio, G., Hultgren, S. J. & Feldman, M. F. Catheterization of mice triggers
838 resurgent urinary tract infection seeded by a bladder reservoir of Acinetobacter baumannii. *Sci*
839 *Transl Med* **15**, eabn8134, doi:10.1126/scitranslmed.abn8134 (2023).
840 44 Meylan, M. *et al.* Tertiary lymphoid structures generate and propagate anti-tumor antibody-
841 producing plasma cells in renal cell cancer. *Immunity*, doi:10.1016/j.immuni.2022.02.001 (2022).
842 45 Goswami, S. *et al.* ARID1A mutation plus CXCL13 expression act as combinatorial biomarkers to
843 predict responses to immune checkpoint therapy in mUCC. *Sci Transl Med* **12**,
844 doi:10.1126/scitranslmed.abc4220 (2020).
845 46 Kroeger, D. R., Milne, K. & Nelson, B. H. Tumor-Infiltrating Plasma Cells Are Associated with
846 Tertiary Lymphoid Structures, Cytolytic T-Cell Responses, and Superior Prognosis in Ovarian
847 Cancer. *Clin Cancer Res* **22**, 3005-3015, doi:10.1158/1078-0432.CCR-15-2762 (2016).
848 47 Pfannstiel, C. *et al.* The Tumor Immune Microenvironment Drives a Prognostic Relevance That
849 Correlates with Bladder Cancer Subtypes. *Cancer Immunol Res* **7**, 923-938, doi:10.1158/2326-
850 6066.CIR-18-0758 (2019).
851 48 Groeneveld, C. S. *et al.* Tertiary lymphoid structures marker CXCL13 is associated with better
852 survival for patients with advanced-stage bladder cancer treated with immunotherapy. *Eur J*
853 *Cancer* **148**, 181-189, doi:10.1016/j.ejca.2021.01.036 (2021).
854 49 Sakimura, C. *et al.* B cells in tertiary lymphoid structures are associated with favorable prognosis
855 in gastric cancer. *J Surg Res* **215**, 74-82, doi:10.1016/j.jss.2017.03.033 (2017).
856 50 Tang, J. *et al.* B Cells and Tertiary Lymphoid Structures Influence Survival in Lung Cancer Patients
857 with Resectable Tumors. *Cancers (Basel)* **12**, doi:10.3390/cancers12092644 (2020).
858 51 Finkin, S. *et al.* Ectopic lymphoid structures function as microniches for tumor progenitor cells in
859 hepatocellular carcinoma. *Nat Immunol* **16**, 1235-1244, doi:10.1038/ni.3290 (2015).
860 52 Figenschau, S. L., Fismen, S., Fenton, K. A., Fenton, C. & Mortensen, E. S. Tertiary lymphoid
861 structures are associated with higher tumor grade in primary operable breast cancer patients.
862 *BMC Cancer* **15**, 101, doi:10.1186/s12885-015-1116-1 (2015).
863 53 Bento, D. C. *et al.* High endothelial venules are rare in colorectal cancers but accumulate in
864 extra-tumoral areas with disease progression. *Oncoimmunology* **4**, e974374,
865 doi:10.4161/2162402X.2014.974374 (2015).

866 54 Jallad, S., Goubet, S., Symes, A., Larner, T. & Thomas, P. Prognostic value of inflammation or
867 granuloma after intravesival BCG in non-muscle-invasive bladder cancer. *BJU Int* **113**, E22-27,
868 doi:10.1111/bju.12334 (2014).
869 55 Pipi, E. *et al.* Tertiary Lymphoid Structures: Autoimmunity Goes Local. *Frontiers in Immunology*
870 **9**, doi:10.3389/fimmu.2018.01952 (2018).
871 56 Zlotta, A. R. *et al.* Humoral response against heat shock proteins and other mycobacterial
872 antigens after intravesical treatment with bacille Calmette-Guerin (BCG) in patients with
873 superficial bladder cancer. *Clin Exp Immunol* **109**, 157-165, doi:10.1046/j.1365-
874 2249.1997.4141313.x (1997).
875 57 Strandgaard, T. *et al.* Elevated T-cell Exhaustion and Urinary Tumor DNA Levels Are Associated
876 with Bacillus Calmette-Guerin Failure in Patients with Non-muscle-invasive Bladder Cancer. *Eur*
877 *Urol* **82**, 646-656, doi:10.1016/j.eururo.2022.09.008 (2022).
878 58 Joudi, F. N., Smith, B. J., O'Donnell, M. A. & Konety, B. R. The Impact of Age on the Response of
879 Patients With Superficial Bladder Cancer to Intravesical Immunotherapy. *Journal of Urology* **175**,
880 1634-1640, doi:10.1016/s0022-5347(05)00973-0 (2006).
881 59 Hinrichs, C. S. *et al.* IL-2 and IL-21 confer opposing differentiation programs to CD8+ T cells for
882 adoptive immunotherapy. *Blood* **111**, 5326-5333, doi:10.1182/blood-2007-09-113050 (2008).
883 60 Marquart, H. V. *et al.* Complement receptor expression and activation of the complement
884 cascade on B lymphocytes from patients with systemic lupus erythematosus (SLE). *Clin Exp*
885 *Immunol* **101**, 60-65, doi:10.1111/j.1365-2249.1995.tb02277.x (1995).
886 61 Krocova, Z. *et al.* The role of B cells in an early immune response to Mycobacterium bovis.
887 *Microb Pathog* **140**, 103937, doi:10.1016/j.micpath.2019.103937 (2020).
888 62 Itoh, Y. *et al.* Four core genotypes mouse model: localization of the Sry transgene and bioassay
889 for testicular hormone levels. *BMC Res Notes* **8**, 69, doi:10.1186/s13104-015-0986-2 (2015).
890 63 Bankhead, P. *et al.* QuPath: Open source software for digital pathology image analysis. *Sci Rep* **7**,
891 16878, doi:10.1038/s41598-017-17204-5 (2017).
892

1A.

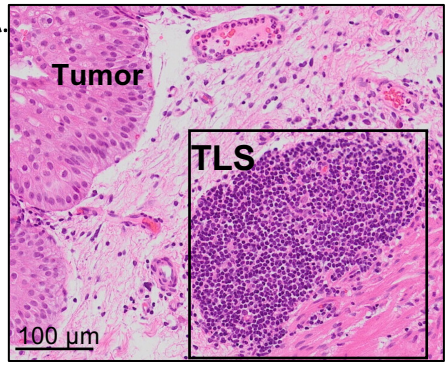

1B

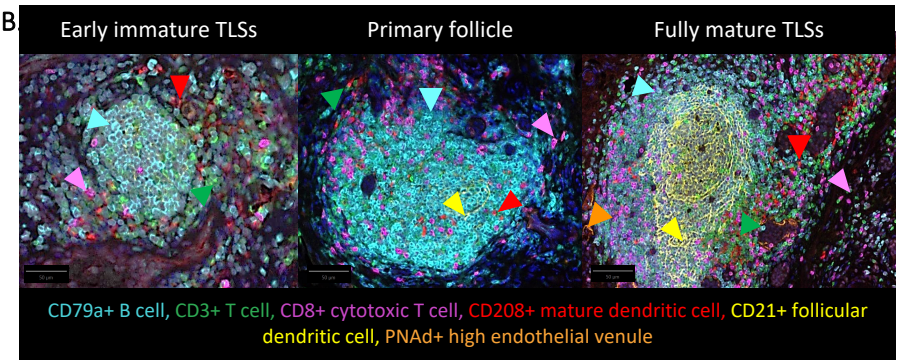

1C.

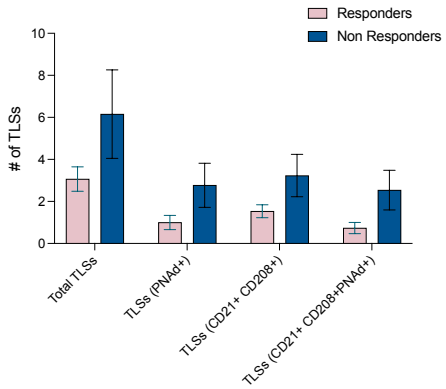

1D.

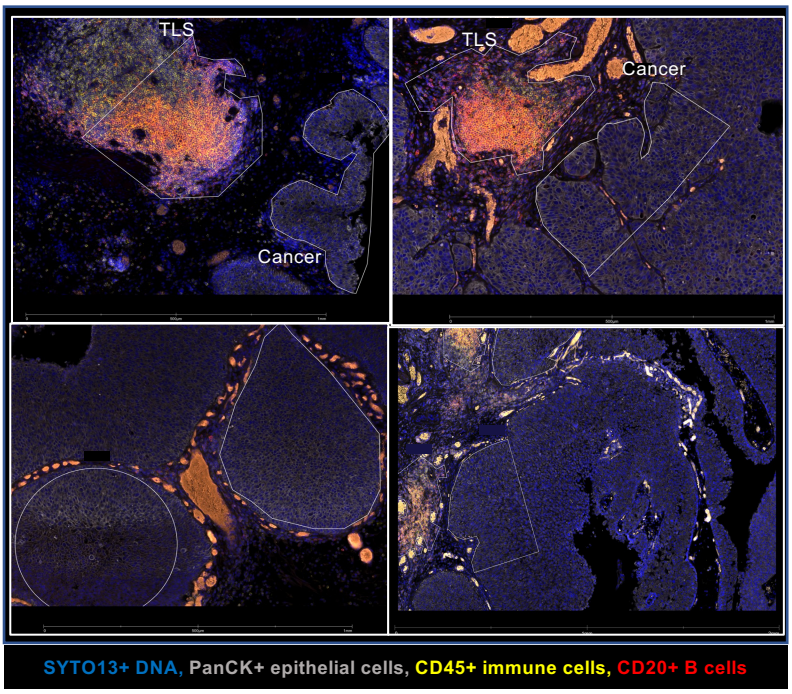

1E.

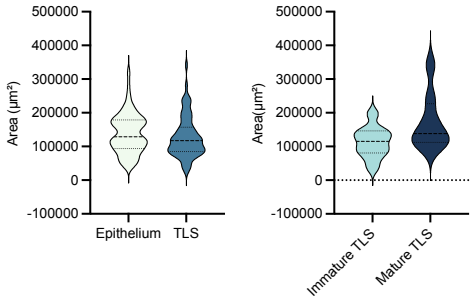

1F.

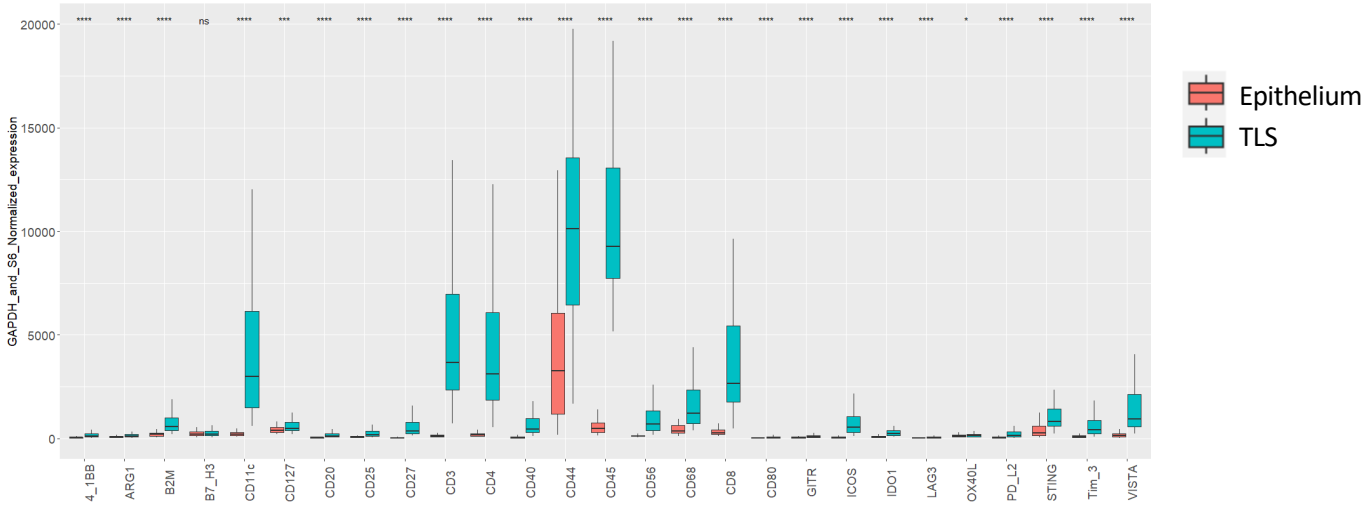

Figure 1. Pre-treatment tumors from BCG non-responders exhibit higher density of tumor adjacent tertiary lymphoid structures. H&E-stained tumor section from a patient classified as BCG non-responder (TLS highlighted in box) (**A**); Classification of different stages of TLSs (identified by expression of CD21+ and CD208+ follicular dendritic cells and PNAd+ high endothelial venules). Multiplex IF showing different stages of TLSs in whole tumor sections (**B**). Bar graph showing higher number of TA-TLSs in BCG non-responders (n=13) compared to responders (n=15) (**C**); Representative images from NanoString GeoMx DSP based staining of 4 whole tumor sections (2 Responders and 2 Non-Responder), showing regions of interest (ROI) selection based on PanCK+/-, CD45+, CD20+ and SYTO 13+ areas/cells (**D**). Violin plot showing area distribution between TLSs and tumor epithelial compartments in all 12 sections (**E**). Box plots showing expression of significantly differentially expressed (*$p<0.05$, ***$p<0.001$, ****$p<0.0001$, ns – not significant) proteins of interest between tumor epithelial regions and TLSs (**F**).

2A.

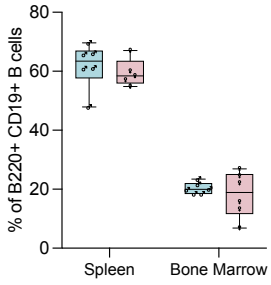

2B.

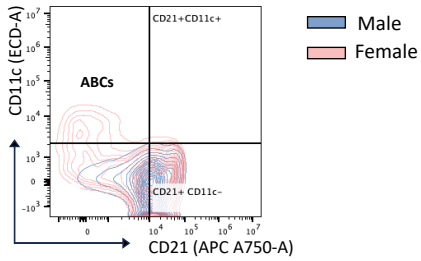

2C.

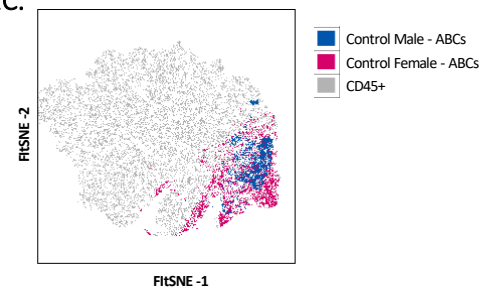

2D.

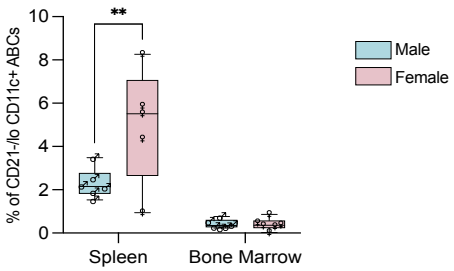

2E.

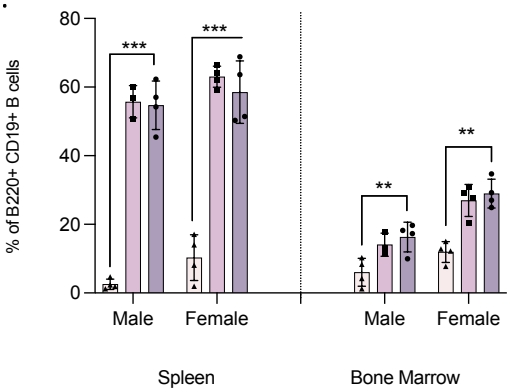

2F.

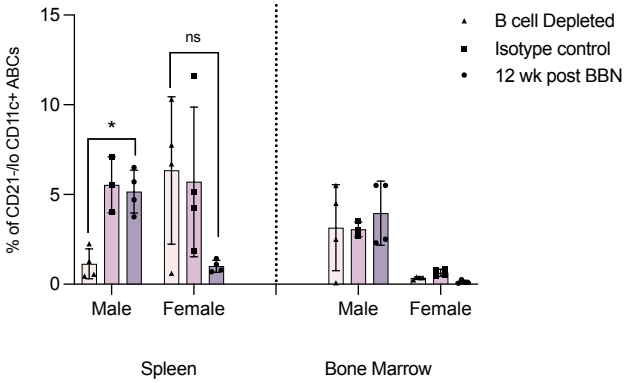

2G.

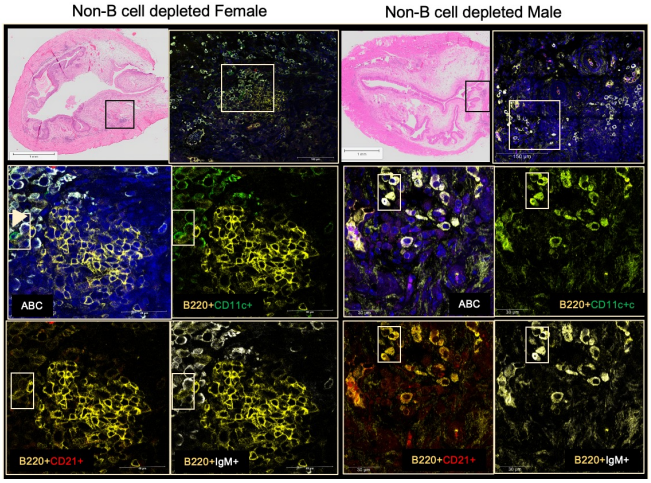

2H.

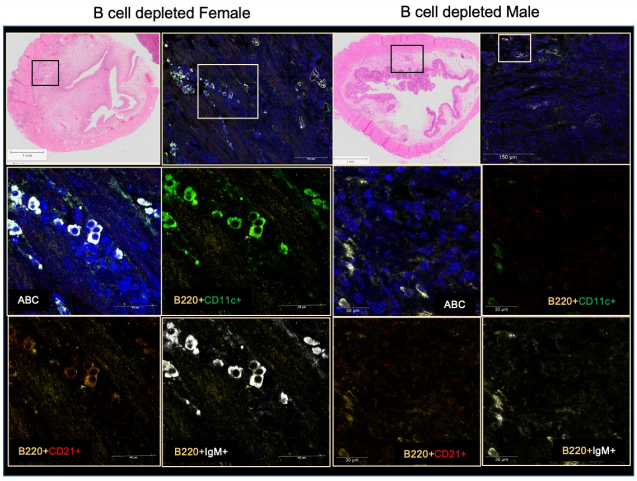

Figure 2. Atypical B cells exhibit sex differences in healthy and carcinogen exposed aging C57BL/6 mice. Comparison of profiles of total B cells (B220+ CD19+) (**A**; n=5-6) and ABCs (CD45+B220+CD19+CD21-/lo CD11c+) (**D**; n=5-6) in spleen and bone marrow of healthy 12-month-old female and male mice. Contour plots and unsupervised Fast interpolation-based t-SNE (FItSNE) plot represents the distribution of ABC population in the total immune (CD45+) cells in healthy male and female mice **(B and C).** FItSNE plot was created using plug-in tool FItSNE and FlowSOM in FlowJo® software. Total B cells and ABCs in B cell depleted, isotype control and untreated female and male mice at 12 weeks post BBN initiation (**E and F**; n=3-4 mice/group). Representative multiplex IF images (n=4/group in each sex) showing differences in bladder infiltrating ABCs at 12 weeks post BBN exposure in female and male mice (**G and H**). Analysis of flow cytometry data was performed using FlowJo® software. All statistical analysis was performed using GraphPad Prism. Ordinary one-way ANOVA with Tukey's post-hoc test was applied to determine statistical significance in differences (*$p<0.05$, **$p < 0.01$, ***$p <0.001$, ns – not significant). Bar graphs represent mean ± SD.

3A.

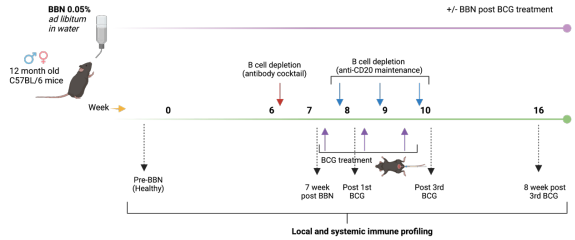

3B. Pre-BBN Week 1

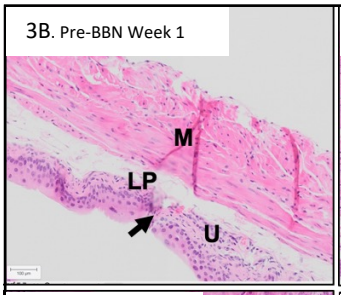

3C. Week 7

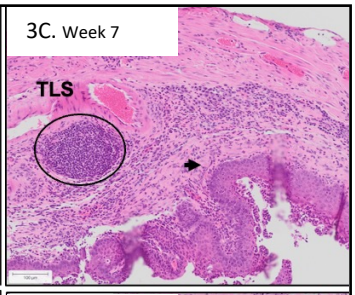

3D. Post 1st BCG

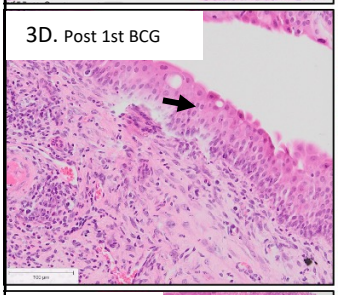

3E. Post 3rd BCG

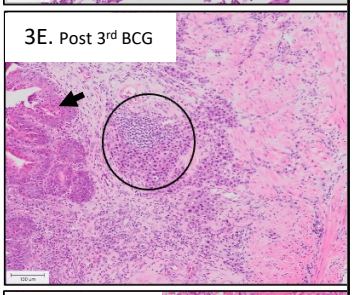

3F. Week 14

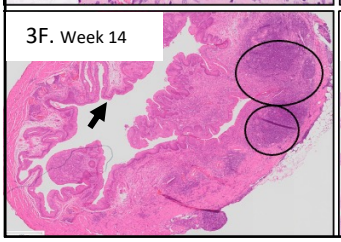

3G. Week 16

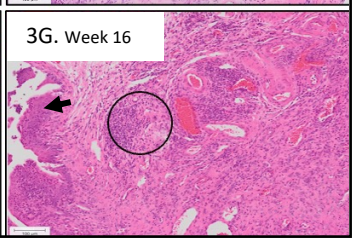

3H.

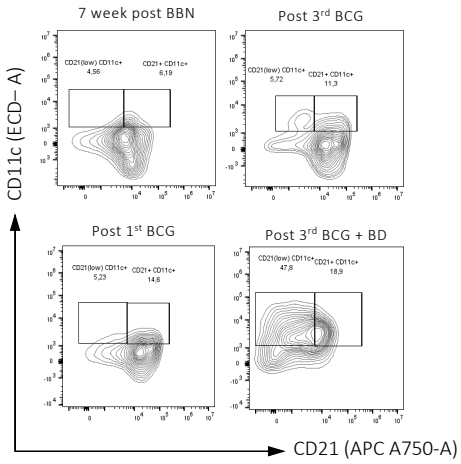

3I.

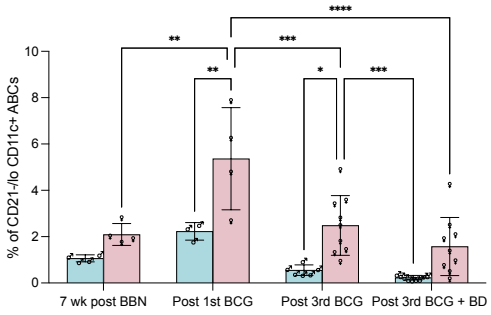

3J.

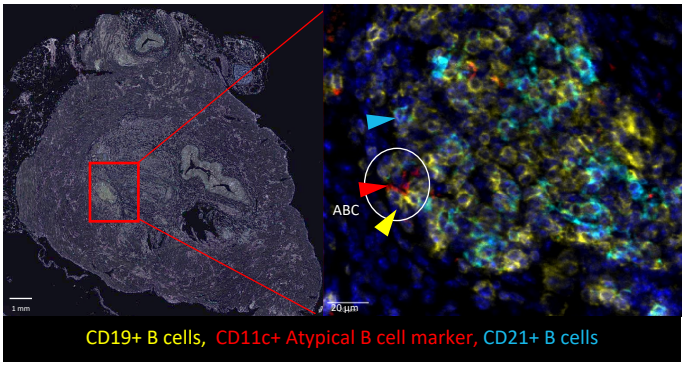

3K.

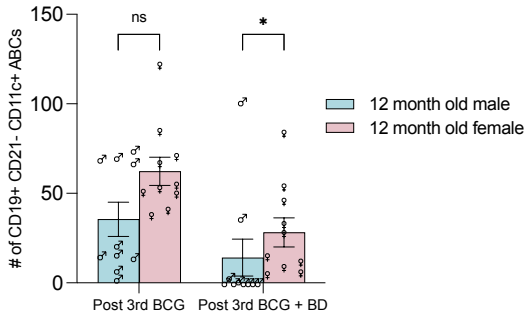

Figure 3. Repeated weekly BCG treatment in aging mice promotes expansion of ABCs and disease progression. Schematic diagram showing experimental approach for intravesical BCG treatment (3 weekly doses) with or without B cell depletion in 12-month-old female and male mice **(A)**. H&E-stained sections showing histological changes in the urothelium and bladder microenvironment at various time points pre-BBN **(B)**, post 7-week BBN (**C**), one week post 1st BCG (**D**), one week post 3rd BCG (**E**), and 6 and 8-weeks post 3rd BCG (**F&G**). Circles indicate lymphoid aggregates/TLSs. Black arrows indicate the urothelium of bladder sections. Scale bar in H&E-stained images – 100 µm. Representative contour plots for identification of splenic ABC population at different time points post BBN and BCG treatment. Contour plots are illustrative of frequency of CD19+ cells and may show disparity in density in comparison to bar graph as shown in B cell depleted and post 3rd BCG treatment group **(H)**. Bar graph represents differences in the frequency of ABCs (CD19+ CD21-/low CD11c+) post BBN and BCG treatment at different time points for both male (n=3-9) and female mice (n=4-9) **(I)**. Analysis of flow cytometry data was performed using FlowJo® software. All statistical analysis was performed using GraphPad Prism. Ordinary two-way ANOVA with Tukey's post-hoc test was applied to determine statistical significance in differences (*p<0.05, **p < 0.01, ***p <0.001, ****p<0.0001). Multiplex IF-stained whole bladder sections showing ABCs (CD19+CD21-CD11c+) in 1 week post 3rd BCG treated 12-month-old female mice **(J).** Representative of 8-10 regions per section (n=5/6 mice in each group). Images at 200x magnification. Bar graph represents number of ABCs (CD19+CD21-CD11c+**)** detected in 10 annotations per treatment group of the bladder microenvironment **(K).** Cell detection analysis and classifier to identify different subsets was performed using QuPath software. All statistical analysis was performed using GraphPad Prism. Mann-Whitney test was applied to determine statistical significance in differences (*p<0.05, ns- not significant). Data presented as mean ± SD.

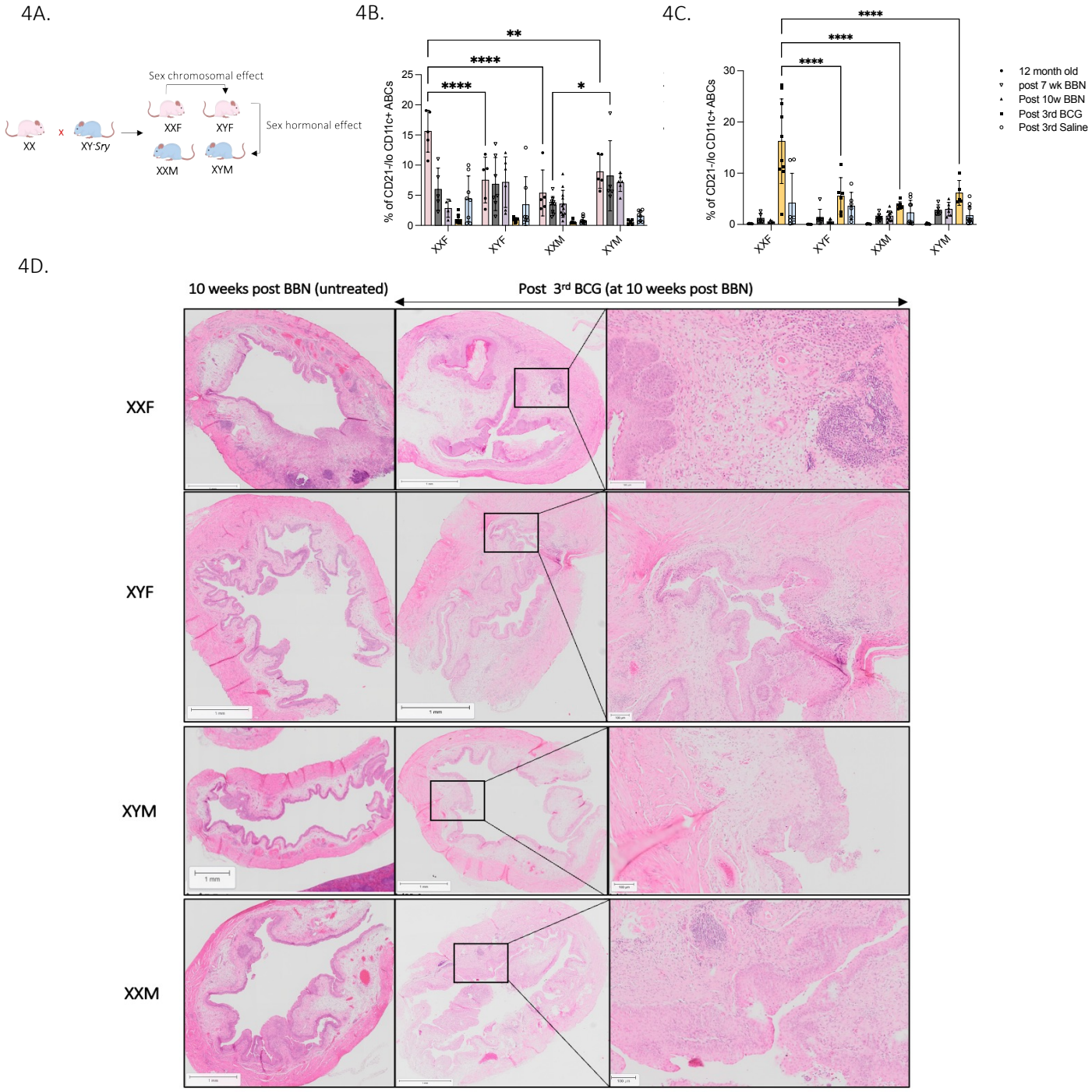

Figure 4. Expansion of ABCs is influenced by hormonal and sex chromosome associated factors. Schematic representation of four core genotype (FCG) mouse model used to study the hormonal and sex chromosomal influence on response to BCG treatment in BBN exposed mice **(A)**. Bar graph showing splenic (**B**) and bone marrow **(C)** CD45+B220+CD19+CD21-/low CD11c+ ABCs in healthy 12-month-old FCG mice; at 10-weeks post BBN and at 1 week post 3rd BCG instillation in BBN exposed mice (BCG treatment initiated at week 7 post BBN initiation). Immune cell frequency was determined using multiparametric flow cytometry. H&E-stained bladder sections from all four genotypes of FCG mice showing differences in bladder microenvironment and overall immune cell infiltration under untreated and BCG treated BBN exposed conditions **(D)**. GraphPad software was used to determine statistically significant differences in profiles across the different genotypes using two-way ANOVA with Bonferroni's test. (*p<0.05, **p<0.001, ****p<0.0001). Statistical comparison (p value) among different groups shown in **Suppl. Table S8.** Data shown as mean ± SD. N=3-9 per group. Scale bar in H&E-stained images – 100 µm.

5A.

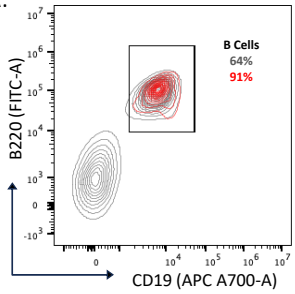

Total splenocytes

B cells - post isolation

5B.

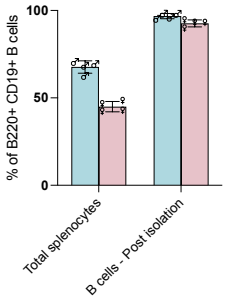

5C.

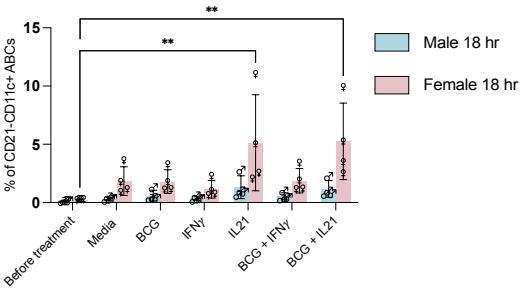

5D.

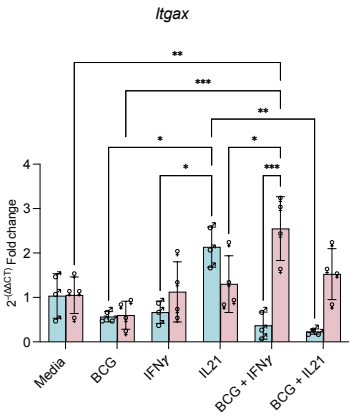

5E.

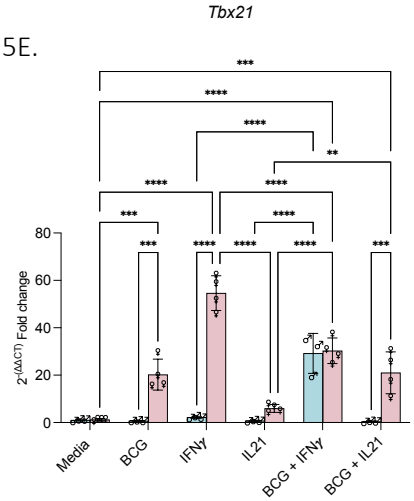

5F.

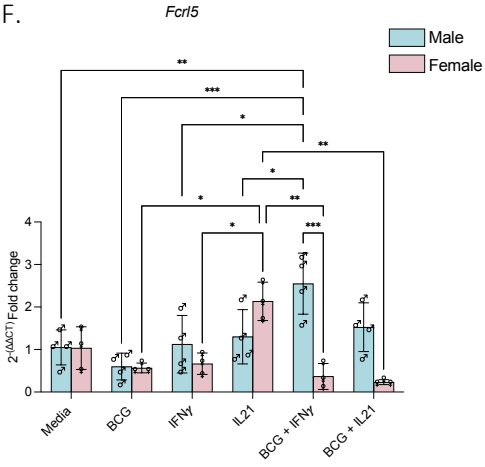

5G.

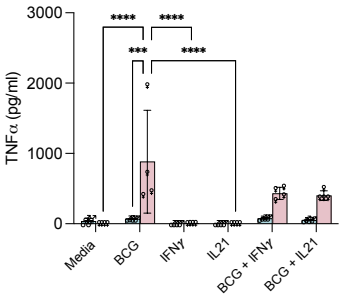

5H.

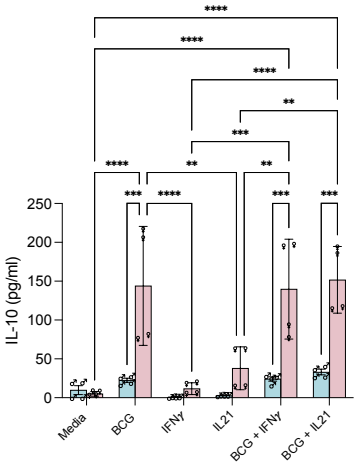

5I.

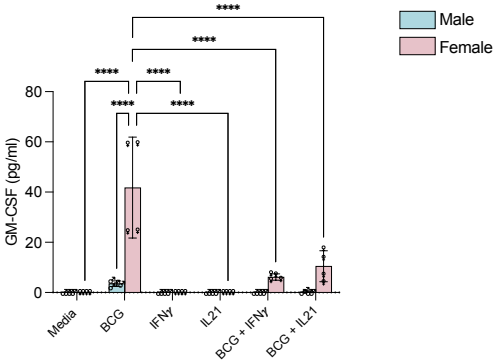

5J.

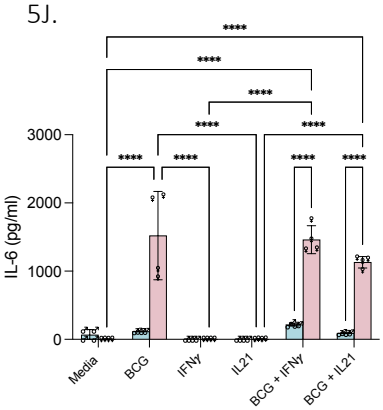

5K.

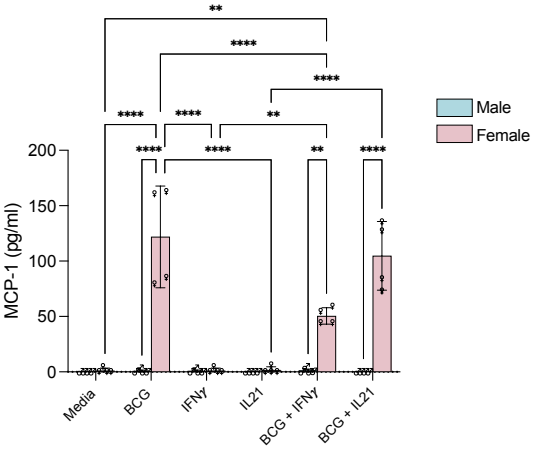

Figure 5. BCG infection and exposure of B cells to IFN-γ and IL-21 increases differentiation of B cells to ABCs in a sex differential manner. Representative contour plot for identification of B220+ CD19+ total splenic B cells before and after enrichment **(A)**. Bar graph illustrates the purity of B cells (93.4 ± 2.2%) after isolation from 12-month-old male and female mice exposed to 7 weeks of BBN **(B).** Bar graph showing increase in ABCs (CD19+ CD21- CD11c+) after 18 h of incubation with IL-21 with or without BCG infection (**C**). Bar graph represents the *Ubc* house keeping gene-normalized $2^{-\Delta\Delta Ct}$ fold change expression levels of ABC-associated genes *Itgax* (**A**)*, Tbx21* (**B**), and *Fcrl5* (**C**) genes in splenic B cells of BBN exposed male and female mice, at 6 h post treatment with IFN-γ, IL-21 in the presence or absence of BCG bacteria. Bar graphs showing significantly increased levels of TNF-α (**D**), IL-10 (**E**), GM-CSF (**F**), IL-6 **(G**) and MCP-1 (**H**) in the supernatants collected at 18 hours post incubation of B cells from female mice compared to those from male mice. B cells were treated with IFN- γ, IL-21 with and without infection with BCG and subjected to multiplex cytokine profiling. GraphPad software was used to determine statistically significant differences in profiles across the different genotypes using two-way ANOVA with Tukey's post hoc test. (*p<0.05, **p<0.001, ****p<0.0001). N=3-4 per group. Data shown as mean ± SD.

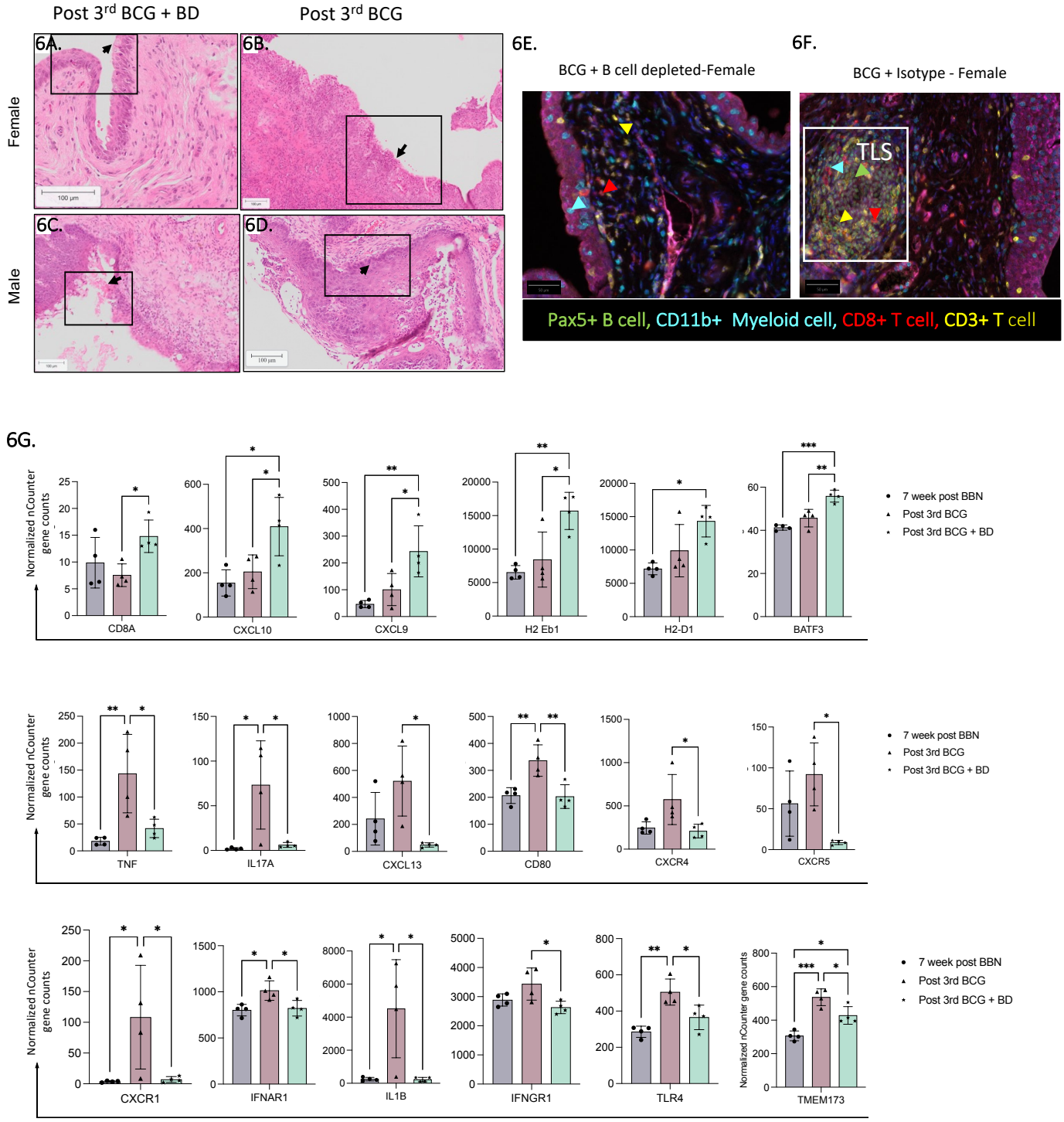
Post 3rd BCG + BD
Post 3rd BCG
Female
Male
6A.
6B.
6C.
6D.
6E.
BCG + B cell depleted-Female
6F.
BCG + Isotype - Female
TLS
Pax5+ B cell, CD11b+ Myeloid cell, CD8+ T cell, CD3+ T cell
6G.
Normalized nCounter gene counts
CD8A
CXCL10
CXCL9
H2 Eb1
H2-D1
BATF3
TNF
IL17A
CXCL13
CD80
CXCR4
CXCR5
CXCR1
IFNAR1
IL1B
IFNGR1
TLR4
TMEM173
7 week post BBN
Post 3rd BCG
Post 3rd BCG + BD

Figure. 6. Effect of transient B cell depletion during BCG treatment on urothelium of BBN exposed female and male mice. H&E-stained whole bladder section showing benign/normal histology of urothelium (shown by arrow) post 3rd BCG + B cell depletion in female **(A)** and focal hyperplasia in male **(C)** mice compared to dysplasia and CIS post 3rd BCG treatment in female **(B)** and male **(D)** mice. Multiplex IF stained whole bladder section showing dysplasia and TLS formation (white box) post 3rd BCG instillation in BCG+ isotype treated **(F)** compared to the BCG+ B cell depleted female mice **(E)**. Representative of 8-10 regions/section, 200x magnification (n=5/6 mice/group). Scale bar in H&E-stained images– 100 µm. Bar graph illustrating the mean ± SD of normalized nCounter gene counts (as indicated), analyzed using NanoString nSolver software. Changes in the expression profiles of selected set of genes in fresh frozen bladders from female mice at 7-weeks post BBN exposure, and one week post 3rd BCG with or without B cell depletion (**G**). Statistical analysis was conducted using GraphPad software with a one-way ANOVA test to identify significant differences in expression profiles across the various genotypes (*$p<0.05$, **$p<0.001$). N=4 per group.

7A.

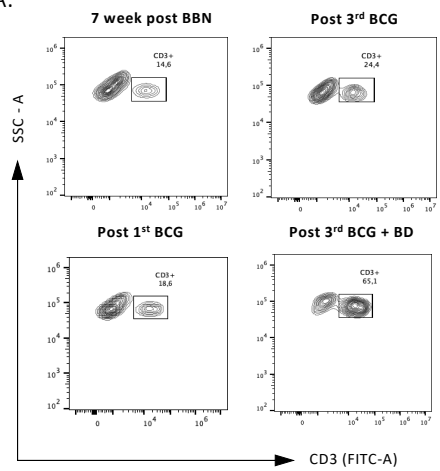
7 week post BBN
Post 3rd BCG
Post 1st BCG
Post 3rd BCG + BD
SSC - A
CD3 (FITC-A)

7B

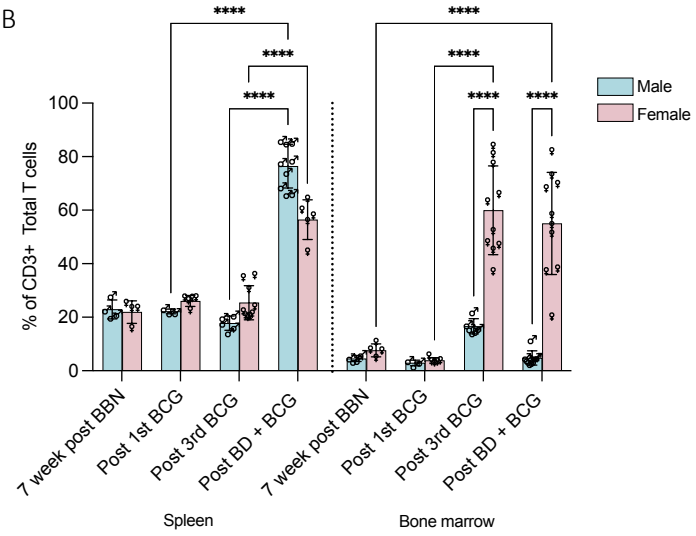
% of CD3+ Total T cells
Male
Female
7 week post BBN
Post 1st BCG
Post 3rd BCG
Post BD + BCG
Spleen
Bone marrow

7C.

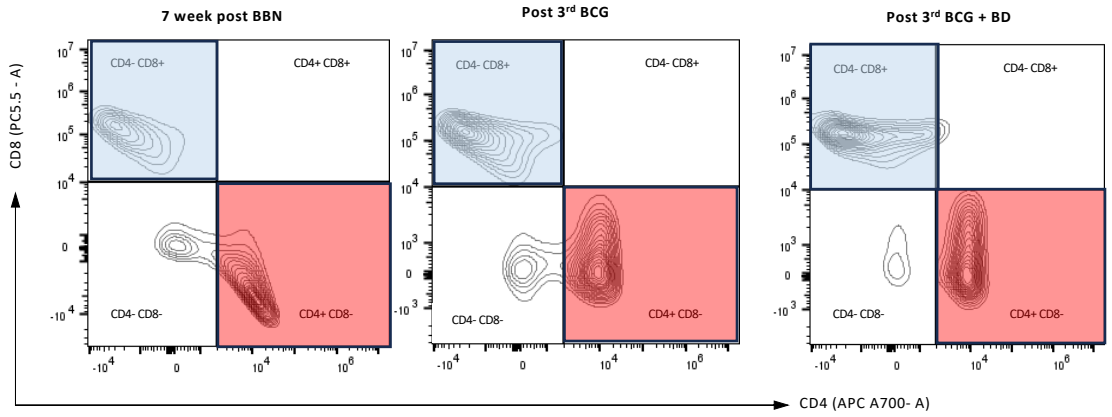
7 week post BBN
Post 3rd BCG
Post 3rd BCG + BD
CD8 (PC5.5 - A)
CD4 (APC A700- A)
CD4- CD8+
CD4+ CD8+
CD4- CD8-
CD4+ CD8-

7D.

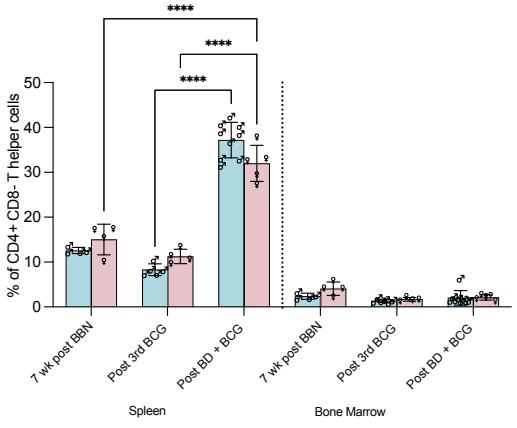
% of CD4+ CD8- T helper cells
7 wk post BBN
Post 3rd BCG
Post BD + BCG
Spleen
Bone Marrow

7E.

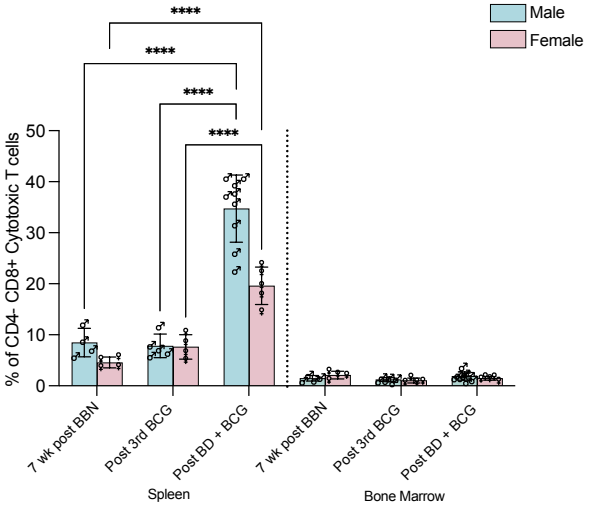
Male
Female
% of CD4- CD8+ Cytotoxic T cells
7 wk post BBN
Post 3rd BCG
Post BD + BCG
Spleen
Bone Marrow

Figure 7. Depletion of B cells during BCG treatment alters systemic T cell profiles in BBN exposed female and male mice. Representative flow cytometry contour plots demonstrating differences in splenic CD45+CD3+ total T cell population in different treatment groups **(A)**. Bar graph represents frequency of total CD3+ T cells in the spleen and bone marrow of 12-month-old male and female C57BL/6 mice at 7-weeks post BBN; one week post 1st BCG; one week post 3rd BCG with or without B cell depletion (**B**). Representative flow cytometry contour plots demonstrating differences in CD4+ CD8- and CD4- CD8+ T cell subsets in different treatment groups **(C).** Bar graph illustrating the variations in the frequency of CD4+ CD8- T helper cells (**D**) and CD4-CD8+ cytotoxic T cells (**E**) in the spleen and bone marrow of 12-month-old aging male and female mice at 7-weeks post BBN; one week post 3rd BCG with or without B cell depletion. Analysis of flow cytometry data was performed using FlowJo® software. All statistical analysis was done in GraphPad Prism software using two-way ANOVA with Bonferroni's test depicted statistical significance. (****$p < 0.0001$). N=3-9 per group. Data presented as mean ± SD.

8A.

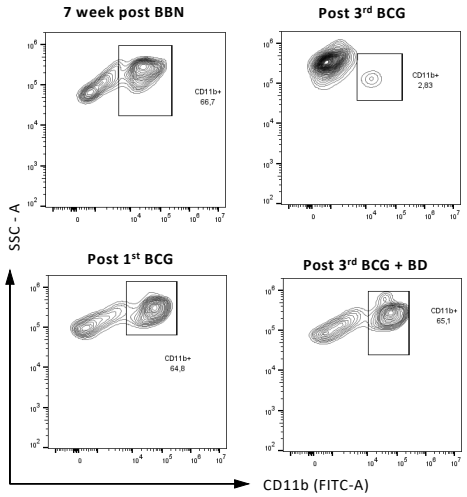

8B.

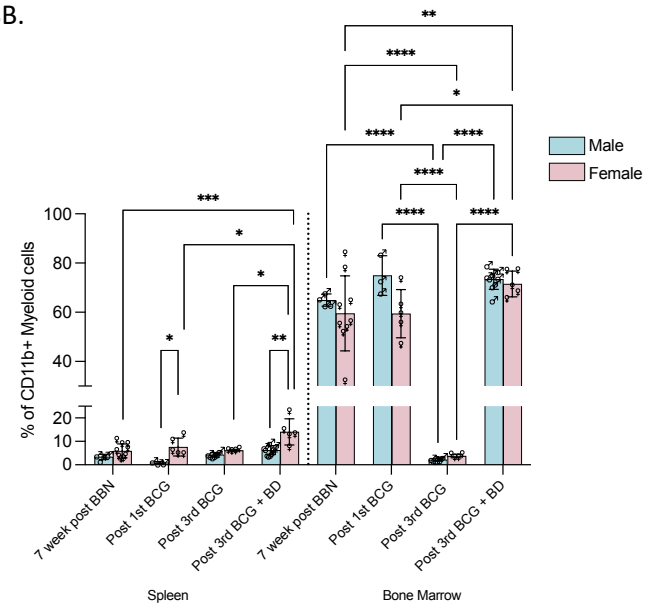

8C.

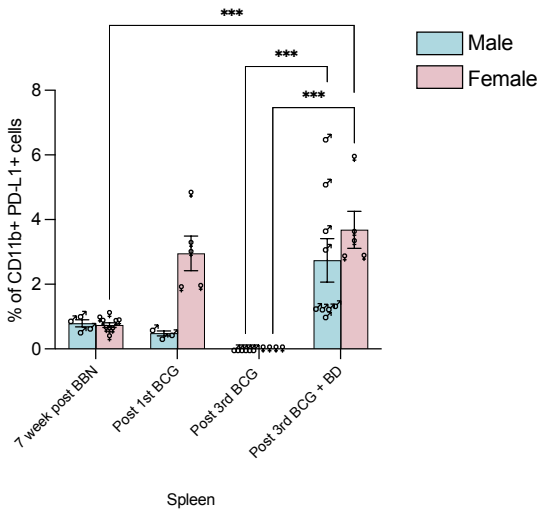

8D.

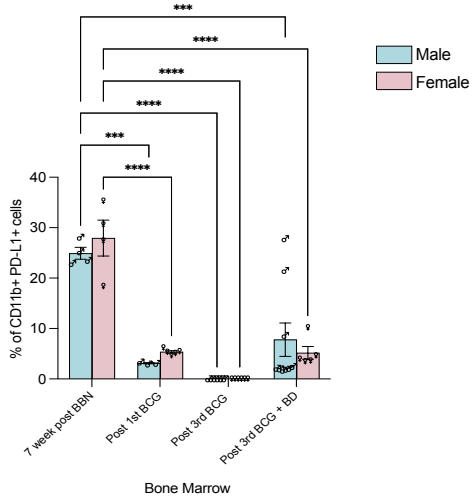

8E.

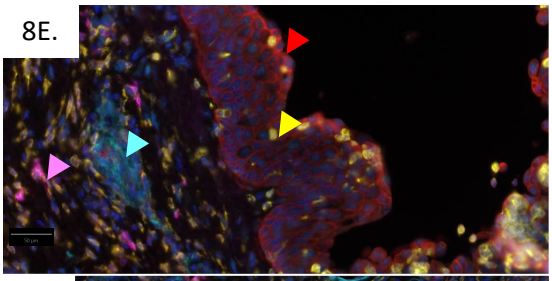

8F.

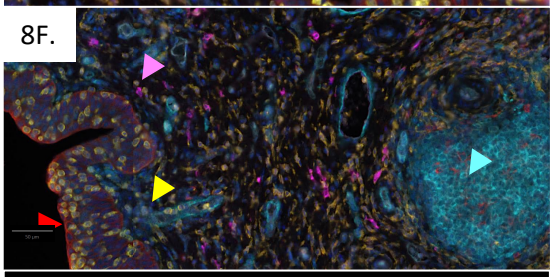

PD-L1+ , F4/80+, CD163+ M2 macrophage, EpCAM+ urothelium

8G.

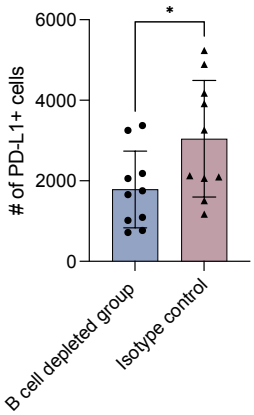

Figure 8. Repeated BCG treatment increases PD-L1 expression on splenic myeloid cells and in the bladder microenvironment. Representative flow cytometry contour plots demonstrating differences in splenic CD45+ CD11b+ total myeloid cell population in different treatment groups **(A)**. Bar graph represents profile of total CD11b+ myeloid cells in the spleen and bone marrow of 12-month-old male and female C57BL/6 mice at 7-weeks post BBN; one week post 1st BCG; one week post 3rd BCG with or without B cell depletion (**B**). Bar graph represents differences in the profile of CD11b+ PD-L1+ cells in spleen **(C)** and bone marrow **(D)** of 12-month-old aging female and male mice at 7-weeks post BBN; one week post 1st BCG; one week post 3rd BCG with or without B cell depletion. Analysis of flow cytometry data was performed using FlowJo® software. All statistical analysis done in GraphPad Prism software (v9.5.1) using two-way ANOVA with Bonferroni's test depicted statistical significance. (*p<0.05, **p<0.01,***p < 0.001,****p < 0.0001). Multiplex IF-stained whole bladder sections showing PD-L1+ cells in BCG + B cell depleted **(E)** and BCG + isotype antibody treated mice **(F)** at 1 week post 3rd BCG instillation. Representative of 8-10 regions per section. Images at 200x magnification. Bar graph (mean ± SD) represents PD-L1+ detections in 10 annotations per treatment group of the bladder section **(G).** Cell detection analysis and classifier to identify PD-L1+ expression was performed using QuPath software. All statistical analysis was performed using GraphPad Prism. Mann-Whitney test was applied to determine statistical significance in differences (*p<0.05). N=3-10 per group. Data presented as mean ± SD.

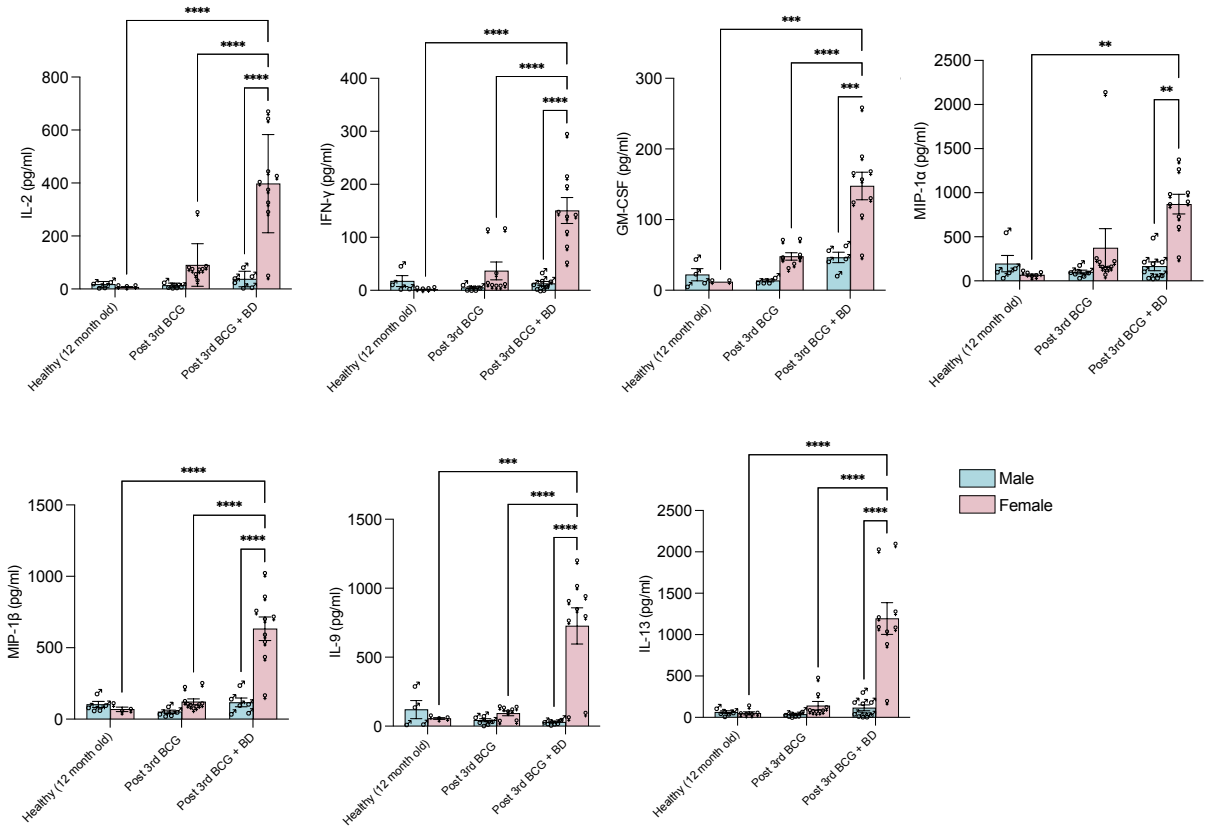

Figure 9. B cell depletion during BCG treatment increases plasma Th1/Th2 cytokine levels. Plasma collected at 1 week post 3rd BCG dose with or without B cell depletion was subjected to multiplex cytokine profiling. Significantly increased levels of Th1 (IL-2, IFN-γ, MIP-1α, MIP-1β), Th2 (IL-9 and IL-13) cytokines and GM-CSF, were observed in BCG+B cell depleted female mice (n=3-4 in each group). All statistical analysis was performed using GraphPad Prism. Statistical significance, *p<0.01, **p<0.001, ***p<0.0001, ****p<0.0001, was determined using two-way ANOVA with Tukey's post-hoc tests. Data presented as mean ± SD.

SUPPLEMENTARY TABLES

Supplementary Table S1. Patient clinical and pathological features

		Responders (n=15)	Non-responders (n=13)
Sex	Male	13 (86.67%)	12 (92.3%)
	Female	2 (13.33%)	1 (7.69%)
Age	50-70 yrs.	7 (46.67%)	8 (61.54%)
	71-90 yrs.	8 (53.3%)	5 (38.4%)
AUA risk category	Low	1 (6.67%)	0 (0.00%)
	Intermediate	7 (46.67%)	4 (30.71%)
	High	7 (46.67%)	9 (69.23%)
Pathology	Non-invasive, Low grade	1 (6.67%)	1 (7.69%)
	CIS	0 (0.00%)	1 (7.69%)
	Non-invasive, High grade	8 (53.3%)	4 (30.76%)
	Invasive, High grade	6 (40%)	7 (53.84%)

Supplementary Table S2. List of proteins investigated via NanoString GeoMx DSP

Immune Cell Profiling Core	IO Drug Target Module	Immune Activation Status Module	Immune Cell Typing Module
Beta-2-microglobulin	4-1BB	CD127	CD45RO
CD11c	LAG3	CD25	FOXP3
CD20	OX40L	CD80	CD34
CD3	Tim-3	ICOS	CD66b
CD4	VISTA	PD-L2	FAP-alpha
CD45	ARG1	CD40	CD14
CD56	B7-H3	CD44	CD163
CD68	IDO1	CD27	
CD8	STING		
CTLA4	GITR		
Fibronectin			
GAPDH			
GZMB			
Histone H3			
HLA-DR			
Ki-67			
Ms IgG1			
Ms IgG2a			
PanCk			
PD-1			
PD-L1			
Rb IgG			
S6			
SMA			

Supplementary Table S3. List of antibodies used in multispectral flow cytometry

ANTIBODIES (B CELL DEPLETION)	SOURCE	IDENTIFIER
Anti-mouse CD19 (Clone 1D3)	Bio X Cell	Cat# BE0150
Anti-mouse CD22 (Clone Cy34.1)	Bio X Cell	Cat# BE0011
Anti-mouse B220 (Clone RA3.3A1/6.1)	Bio X Cell	Cat# BE0067
Anti-mouse CD20 (Clone MB20-11)	Bio X Cell	Cat# BE0356
Anti-rat kappa Immunoglobulin Light Chain (Clone MB20-11)	Bio X Cell	Cat# BE0122
Rat IgG2a Isotype control (Clone 2A3)	Bio X Cell	Cat# BE0089
Mouse IgG1 Isotype control (Clone MOPC-21)	Bio X Cell	Cat# BE0083
Polyclonal rat IgG Isotype control (Clone N/A)	Bio X Cell	Cat# BE0094
Mouse IgG2a Isotype control (Clone C1.18.4)	Bio X Cell	Cat# BE0085
ANTIBODIES (FLOW CYTOMETRY)	**SOURCE**	**IDENTIFIER**
Anti-mouse CD45 – Pacific Blue (Clone 30-F11)	BioLegend	Cat# 103126
Anti-mouse CD19 – Alexa Fluor 700 (Clone 6D5)	BioLegend	Cat# 115528
Anti-mouse CD21 – APC/Cyanine 7 (Clone 7E9)	BioLegend	Cat# 123418
Anti-mouse CD11c – PE/Dazzle 594 (Clone N418)	BioLegend	Cat# 117348
Anti-mouse B220 – FITC (Clone RA3-6B2)	BioLegend	Cat# 103206
Anti-mouse IgD - PE (Clone 11-26c.2a)	BioLegend	Cat# 405705
Anti-mouse CD3ε – FITC (Clone 145-2C11)	BioLegend	Cat# 100306
Anti-mouse CD4 – Alexa Fluor 700 (Clone GK1.5)	BioLegend	Cat# 100430
Anti-mouse CD8a – PE/Fire 700 (Clone 53-6.7)	BioLegend	Cat# 100791
Anti-mouse/rat/human FOXP3- PE (Clone 150D)	BioLegend	Cat# 320008
Anti-mouse CD279 – APC (Clone RMP1-30)	BioLegend	Cat# 109112
Anti-mouse NK-1.1 – Brilliant violet 785 (Clone PK136)	BioLegend	Cat# 108749
Anti-mouse/human CD11b – FITC (Clone M1/70)	BioLegend	Cat# 101206
Anti-mouse F4/80 – PE/Cyanine5 (Clone BM8)	BioLegend	Cat# 123112
Anti-mouse CD274 – PE/Cyanine7 (Clone 10F.9G2)	BioLegend	Cat# 124314
Anti-mouse CD8a – PE (Clone 53-6.7)	BioLegend	Cat# 100708
Purified anti-mouse CD16/32 (Clone 93)	BioLegend	Cat# 101302

Supplementary Table S4. Antibodies used in multiplex IF staining.

Primary Antibody	Staining Round	Species	Cat#	Clone #	Ab Dilution (Diluent)	Fluorophore	Fluorophore dilution
CD208	1	Rat	DDX0191P-100	1010E1.01	1/100 (RR)	Opal 650	1/100
CD3	2	Rabbit	M3074	SP7	1/600 (DVG)	Opal 520	1/300
PNAd	3	Rat	120802	MECA-79	1/200 (DVG)	Opal 620	1/100
Pax5	4	Rabbit	ab109443	EPR3730	1/1000 (DVG)	Opal 540	1/500
CD8	5	Rabbit	98941S	D4W2Z	1/200 (DVG)	Opal 690	1/150
CD11b	6	Rabbit	ab133357	EPR1344	1/7500 (DVG)	Opal 570	1/800
CD163	1	Rabbit	ab182422	EPR19518	1/3000 (RR)	Opal 570	1/200
Ly6G	2	Rat	127607	1A8	1/800 (DVG)	Opal 620	1/300
EpCAM	3	Rabbit	ab221552	EPR20533-63	1/600 (DVG)	Opal 690	1/100
PD-L1	4	Rabbit	64988	D5V3B	1/150 (DVG)	Opal 520	1/100
CD11c	1	Rabbit	97585	D1V9Y	1/200 (DVG)	Opal480	1/100
CD21	3	Rabbit	ab227662	SP186	1/100 (DVG)	Opal620	1/100
CD19	4	Rabbit	90176T	D4V4BXP (R)	1/800 (DVG)	Opal570	1/800

Supplementary Table S5. Antibodies used in atypical B cell panel for multiplex IF staining.

Primary Antibody	Species	Cat#	Clone	Company	Ab Dilution
B220	Rat	14-0452-81	RA3-6B2	ThermoFisher	1:200
CD11c	Armenian Hamster	14-0114-81	N418	ThermoFisher	1:100
IgM	Goat	A90-101A	N/A	Fortis Life Sciences	1:150
CD21	Rabbit	MA5-32227	SC0681	ThermoFisher	1:100
Anti-LAM	Rabbit	MBS320597	N/A	MyBioSource	1:100

Secondary Antibody	**Conjugate**	**Cat#**	**Company**	**Ab Dilution**
Goat anti-Rat	Alexa Fluor 555	A-21434	ThermoFisher	1:400
Goat anti-Armenian hamster	Alexa Fluor 488	ab173003	Abcam	1:250
Donkey anti-Goat	Alexa Fluor 647	A-21447	ThermoFisher	1:200
Donkey anti-Rabbit	Alexa Fluor 594	A-21207	ThermoFisher	1:400

Supplementary Table S6. List of primers used for quantitative RT-PCR

Gene Symbol	Species	Cat#	Company
Aicda	Mouse	4453320	ThermoFisher
Fcrl5	Mouse	4448892	ThermoFisher
Itgax	Mouse	4453320	ThermoFisher
Il10	Mouse	4453320	ThermoFisher
Tbx21	Mouse	4453320	ThermoFisher
Tlr7	Mouse	4448892	ThermoFisher
Tlr9	Mouse	4453320	ThermoFisher
Ubc	Mouse	4453320	ThermoFisher

Supplementary Table S7. List of genes investigated via NanoString nCounter

ATG5	*CXCL9*	*H2-D1*	*IL17RA*	*PDCD1*
BATF3	*CXCR3*	*H2-DMb1*	*IL1B*	*PDIA3*
BAX	*Cd63*	*H2-Dma*	*IL1R1*	*PIK3CA*
Bcl6	*Cxcl13*	*H2-Eb1*	*IL6*	*PRF1*
CALR	*Cxcr1*	*H2-K1*	*Icos*	*PSMB9*
CASP1	*Cxcr4*	*HMGB1*	*Irf4*	*SF3A3*
CASP8	*Cxcr5*	*HSP90AA1*	*Isg15*	*STAT1*
CCL5	*E2-2*	*IDO1*	*Klrb1c*	*STAT3*
CD274	*EIF2AK3*	*IFNA1*	*Klrk1*	*Sap130*
CD4	*ENTPD1*	*IFNAR1*	*LY96*	*Sdha*
CD80	*Edc3*	*IFNB1*	*MYD88*	*Siglech*
CD86	*FOXP3*	*IFNG*	*Mavs*	*TLR4*
CD8A	*Gusb*	*IFNGR1*	*NLRP3*	*TMEM173*
CD8B	*H2-Aa*	*IL10*	*NT5E*	*TNF*
CXCL10	*H2-Ab1*	*IL17A*	*P2RX7*	*cd81*

Supplementary Table S8. Summary of statistical comparison of splenic ABC profiles between the treatment groups of the four genotypes of FCG

Comparison group	Summary	Individual p value	Comparison group	Summary	Individual p value
XXF:12 month old vs. XXF:Post 7 wk BBN	****	<0.0001	XXF:Post 10 wk BBN vs. XYM:12 month old	**	0.0017
XXF:12 month old vs. XXF:Post 10 wk BBN	****	<0.0001	XXF:Post 10 wk BBN vs. XYM:post 7 wk BBN	**	0.0052
XXF:12 month old vs. XXF:Post 3rd BCG	****	<0.0001	XXF:Post 10 wk BBN vs. XYM:Post 10 wk BBN	*	0.0208
XXF:12 month old vs. XXF:Post 3rd Saline	****	<0.0001	XXF:Post 3rd BCG vs. XXF:Post 3rd Saline	*	0.0116
XXF:12 month old vs. XYF:12 month old	****	<0.0001	XXF:Post 3rd BCG vs. XYF:12 month old	****	<0.0001
XXF:12 month old vs. XYF:post 7 wk BBN	****	<0.0001	XXF:Post 3rd BCG vs. XYF:post 7 wk BBN	****	<0.0001
XXF:12 month old vs. XYF:Post 10 wk BBN	****	<0.0001	XXF:Post 3rd BCG vs. XYF:Post 10 wk BBN	****	<0.0001
XXF:12 month old vs. XYF:Post 3rd BCG	****	<0.0001	XXF:Post 3rd BCG vs. XXM:12 month old	**	0.0053
XXF:12 month old vs. XYF:Post 3rd Saline	****	<0.0001	XXF:Post 3rd BCG vs. XXM:Post 10 wk BBN	*	0.0354
XXF:12 month old vs. XXM:12 month old	****	<0.0001	XXF:Post 3rd BCG vs. XYM:12 month old	****	<0.0001
XXF:12 month old vs. XXM:post 7 wk BBN	****	<0.0001	XXF:Post 3rd BCG vs. XYM:post 7 wk BBN	****	<0.0001
XXF:12 month old vs. XXM:Post 10 wk BBN	****	<0.0001	XXF:Post 3rd BCG vs. XYM:Post 10 wk BBN	****	<0.0001
XXF:12 month old vs. XXM:Post 3rd BCG	****	<0.0001	XXF:Post 3rd Saline vs. XYF:Post 3rd BCG	*	0.0227
XXF:12 month old vs. XXM:Post 3rd Saline	****	<0.0001	XXF:Post 3rd Saline vs. XXM:Post 3rd BCG	**	0.0086
XXF:12 month old vs. XYM:12 month old	***	0.0003	XXF:Post 3rd Saline vs. XXM:Post 3rd Saline	**	0.0091
XXF:12 month old vs. XYM:post 7 wk BBN	****	<0.0001	XXF:Post 3rd Saline vs. XYM:12 month old	**	0.0061
XXF:12 month old vs. XYM:Post 10 wk BBN	****	<0.0001	XXF:Post 3rd Saline vs. XYM:post 7 wk BBN	*	0.0196
XXF:12 month old vs. XYM:Post 3rd BCG	****	<0.0001	XXF:Post 3rd Saline vs. XYM:Post 3rd BCG	*	0.0170
XXF:12 month old vs. XYM:Post 3rd Saline	****	<0.0001	XXF:Post 3rd Saline vs. XYM:Post 3rd Saline	*	0.0450
XXF:post 7 wk BBN vs. XXF:Post 3rd BCG	**	0.0015	XYF:12 month old vs. XYF:Post 3rd BCG	***	0.0002
XXF:post 7 wk BBN vs. XYF:Post 3rd BCG	**	0.0034	XYF:12 month old vs. XYF:Post 3rd Saline	*	0.0155
XXF:post 7 wk BBN vs. XXM:Post 3rd BCG	**	0.0012	XYF:12 month old vs. XXM:post 7 wk BBN	**	0.0094
XXF:post 7 wk BBN vs. XXM:Post 3rd Saline	**	0.0012	XYF:12 month old vs. XXM:Post 10 wk BBN	**	0.0095
XXF:post 7 wk BBN vs. XYM:Post 3rd BCG	**	0.0026	XYF:12 month old vs. XXM:Post 3rd BCG	****	<0.0001
XXF:post 7 wk BBN vs. XYM:Post 3rd Saline	**	0.0066	XYF:12 month old vs. XXM:Post 3rd Saline	****	<0.0001
XXF:Post 10 wk BBN vs. XYF:12 month old	*	0.0149	XYF:12 month old vs. XYM:Post 3rd BCG	***	0.0002
XXF:Post 10 wk BBN vs. XYF:post 7 wk BBN	*	0.0250	XYF:12 month old vs. XYM:Post 3rd Saline	***	0.0003
XXF:Post 10 wk BBN vs. XYF:Post 10 wk BBN	*	0.0190	XYF:post 7 wk BBN vs. XYM:Post 3rd BCG	*	0.0117
XYF:post 7 wk BBN vs. XXM:post 7 wk BBN	*	0.0155	XYF:post 7 wk BBN vs. XYM:Post 3rd Saline	*	0.0118
XYF:post 7 wk BBN vs. XXM:Post 10 wk BBN	*	0.0156	XYF:Post 10 wk BBN vs. XYF:Post 3rd BCG	****	<0.0001
XYF:post 7 wk BBN vs. XXM:Post 3rd BCG	****	<0.0001	XYF:Post 10 wk BBN vs. XYF:Post 3rd Saline	****	<0.0001
XYF:post 7 wk BBN vs. XXM:Post 3rd Saline	****	<0.0001	XYF:Post 3rd BCG vs. XXM:12 month old	*	0.0100
XYF:Post 10 wk BBN vs. XYM:Post 3rd BCG	***	0.0002	XYF:Post 3rd BCG vs. XYM:12 month old	****	<0.0001
XYF:Post 10 wk BBN vs. XYM:Post 3rd Saline	***	0.0004	XYF:Post 3rd BCG vs. XYM:post 7 wk BBN	****	<0.0001
XYF:Post 3rd Saline vs. XYM:12 month old	**	0.0013	XYF:Post 3rd BCG vs. XYM:Post 10 wk BBN	***	0.0002
XYF:Post 3rd Saline vs. XYM:post 7 wk BBN	**	0.0046	XXM:12 month old vs. XXM:Post 3rd BCG	**	0.0039
XYF:Post 3rd Saline vs. XYM:Post 10 wk BBN	*	0.0219	XXM:12 month old vs. XXM:Post 3rd Saline	**	0.0042
XXM:12 month old vs. XYM:Post 3rd BCG	**	0.0076	XXM:12 month old vs. XYM:12 month old	*	0.0499
XXM:12 month old vs. XYM:Post 3rd Saline	*	0.0193	XXM:post 7 wk BBN vs. XXM:Post 3rd BCG	*	0.0378
XXM:Post 10 wk BBN vs. XXM:Post 3rd BCG	*	0.0252	XXM:post 7 wk BBN vs. XXM:Post 3rd Saline	*	0.0430
XXM:Post 10 wk BBN vs. XXM:Post 3rd Saline	*	0.0277	XXM:post 7 wk BBN vs. XYM:12 month old	***	0.0006
XXM:Post 10 wk BBN vs. XYM:12 month old	***	0.0005	XXM:post 7 wk BBN vs. XYM:post 7 wk BBN	**	0.0024
XXM:Post 10 wk BBN vs. XYM:post 7 wk BBN	**	0.0024	XXM:post 7 wk BBN vs. XYM:Post 10 wk BBN	*	0.0131
XXM:Post 10 wk BBN vs. XYM:Post 10 wk BBN	*	0.0133	XXM:Post 3rd BCG vs. XYM:12 month old	****	<0.0001
XXM:Post 10 wk BBN vs. XYM:Post 3rd BCG	*	0.0458	XXM:Post 3rd BCG vs. XYM:post 7 wk BBN	****	<0.0001
XYM:12 month old vs. XYM:Post 3rd BCG	****	<0.0001	XXM:Post 3rd BCG vs. XYM:Post 10 wk BBN	****	<0.0001
XYM:12 month old vs. XYM:Post 3rd Saline	****	<0.0001	XYM:post 7 wk BBN vs. XYM:Post 3rd Saline	****	<0.0001
XYM:post 7 wk BBN vs. XYM:Post 3rd BCG	****	<0.0001	XXM:Post 3rd Saline vs. XYM:12 month old	****	<0.0001
XYM:Post 10 wk BBN vs. XYM:Post 3rd BCG	***	0.0002	XXM:Post 3rd Saline vs. XYM:post 7 wk BBN	****	<0.0001
XYM:Post 10 wk BBN vs. XYM:Post 3rd Saline	***	0.0004	XXM:Post 3rd Saline vs. XYM:Post 10 wk BBN	****	<0.0001